Potential-functional embedding theory for molecules and materials

Chen Huang and Emily A. Carter

Articles you may be interested in

Time-dependent potential-functional embedding theory
J. Chem. Phys. **140**, 124113 (2014); 10.1063/1.4869538

Understanding the role of ions and water molecules in the NaCl dissolution process
J. Chem. Phys. **139**, 234702 (2013); 10.1063/1.4840675

Size-dependent structures of Na n I n 1 + cluster ions with a methanol adsorbate: A combined study by photodissociation spectroscopy and density-functional theory calculation
J. Chem. Phys. **123**, 161101 (2005); 10.1063/1.2102909

Linear scaling computation of the Fock matrix. VII. Periodic density functional theory at the point
J. Chem. Phys. **122**, 134102 (2005); 10.1063/1.1853374

Density functional study of endohedral complexes M@C 60 (M=Li , Na, K, Be, Mg, Ca, La, B, Al): Electronic properties, ionization potentials, and electron affinities
J. Chem. Phys. **108**, 3498 (1998); 10.1063/1.475783

Re-register for Table of Content Alerts

Create a profile.

Sign up today!

Potential-functional embedding theory for molecules and materials

Chen Huang[1] and Emily A. Carter[2,a)]

[1]*Department of Physics, Princeton University, Princeton, New Jersey 08544, USA*
[2]*Department of Mechanical and Aerospace Engineering, Program in Applied and Computational Mathematics, and the Andlinger Center for Energy and the Environment, Princeton University, Princeton, New Jersey 08544-5263, USA*

We introduce a potential-functional embedding theory by reformulating a recently proposed density-based embedding theory in terms of functionals of the embedding potential. This potential-functional based theory completes the dual problem in the context of embedding theory for which density-functional embedding theory has existed for two decades. With this potential-functional formalism, it is straightforward to solve for the unique embedding potential shared by all subsystems. We consider charge transfer between subsystems and discuss how to treat fractional numbers of electrons in subsystems. We show that one is able to employ different energy functionals for different subsystems in order to treat different regions with theories of different levels of accuracy, if desired. The embedding potential is solved for by directly minimizing the total energy functional, and we discuss how to efficiently calculate the gradient of the total energy functional with respect to the embedding potential. Forces are also derived, thereby making it possible to optimize structures and account for nuclear dynamics. We also extend the theory to spin-polarized cases. Numerical examples of the theory are given for some homo- and hetero-nuclear diatomic molecules and a more complicated test of a six-hydrogen-atom chain. We also test our theory in a periodic bulk environment with calculations of basic properties of bulk NaCl, by treating each atom as a subsystem. Finally, we demonstrate the theory for water adsorption on the MgO(001)surface. © *2011 American Institute of Physics*. [doi:10.1063/1.3659293]

I. INTRODUCTION

Accurate and detailed electronic properties and energies are a prerequisite for proper understanding and reliable prediction of material properties on a variety of length scales. Theories of varying levels of accuracy exist in the literature. Correlated-wavefunction (CW) theories include in their canon formally exact means for solving the many-body Schrödinger equation (full configuration interaction (CI)). However, the computational cost of CW theories tends to scale dramatically with respect to the system's size. Even though (quasi-) linear-scaling CW methods[1] have been introduced in the last 10 years; it is still not feasible to apply these highly accurate methods to systems that contain hundreds of atoms. On the other hand, Kohn-Sham density functional theory (KS-DFT),[2] which is based on the Hohenberg-Kohn[3] (HK) DFT, greatly simplifies solving the many-body Schrödinger equation by introducing the fictitious KS non-interacting electrons and grouping most of the many-body information into the so-called exchange-correlation functionals (XCs). In principle, KS-DFT is exact and its accuracy can be improved by using more advanced XC functionals,[4,5] such as orbital-dependent XC functionals. However, these latter functionals again require considerable computational time. Unfortunately, the most common implementations of KS-DFT cannot adequately address many problems in material

and life sciences, such as van der Waals interactions between polymer strands, strong correlations in transition metal and rare earth ionic compounds, adsorption of some molecules on metal surfaces, singlet diradicals, etc. For these problems, CW methods generally provide superior predictions.

The near-sightedness principle[6] renders valid the application of a theory of high accuracy to a local region of interest while treating the rest of the quantum system with a more approximate theory that requires much less computational effort. One example[7,8] from surface science is to use a CI description for an adsorbate and nearby surface atoms (a cluster), with the rest of the surface (the environment) treated, e.g.*,* within KS-DFT. An embedding theory is needed to describe the interaction between the cluster and its environment. Different embedding schemes exist for different scenarios. In ionic solids, usually the environment is modeled sufficiently accurately with an extended point charge array. If the polarization of the environment is also important, a more sophisticated classical shell-model[9] can be used. Another approach is the *ab initio* model potential method,[10] which delivers *ab initio* embedding potentials that have been used to study local geometries, excitation spectra, etc. for defects in ionic solids. In covalently-bonded solids and in large molecules, the covalent bonds are usually cut and saturated with pseudo-hydrogen atoms.[11] For metallic systems, density-based embedding is usually preferable, since the delocalization of electrons cannot be handled by embedding theories[10,11] designed for ionic or covalent solids. Density-based embedding is based on the partitioning of the total

---

a)Author to whom correspondence should be addressed. Electronic mail: eac@princeton.edu.

electron density into subsystems, as a choice for fast KS-DFT calculations[12,13] and DFT-in-DFT embedding schemes.[14] It was then extended by Carter and co-workers[15,16] for embedded CW calculations. In principle, density-based embedding, which is based on DFT, is formally exact. A recent review of embedding schemes is available.[17]

Ultimately, a successful embedding theory should attempt to satisfy a number of requirements. (1) It should be able to treat the long-range electrostatic interactions between the cluster and its environment in a self-consistent fashion, which means that the cluster's and environment's electron distributions adjust to each other until they reach an equilibrium state. This will be important for cases in which the cluster and environment are easily polarized. (2) The embedding theory should be able to accurately describe the short-range interaction at the boundary between the cluster and its environment. In density-based embedding theory, these short-range terms largely involve partitioning of kinetic energy and XC terms.[7,8,15–17] (3) The theory should be able to equilibrate the chemical potential between the cluster and its environment by allowing charge transfer between the two. For density-based embedding, we have an additional requirement: (4) since multiple ways exist to partition the total electron density into a cluster and its environment,[8] the embedding theory should have a unique partitioning of the total electron density to make the theory tractable.

The fourth requirement has been analyzed in detail in the partition-density functional theory (PDFT) (Refs. 18–21) and our recent density-based embedding theory.[8] In these theories, the non-uniqueness of density partitioning is removed by applying a constraint that the embedding potential is the same for all subsystems. Charge redistribution among subsystems (the third point above) was also discussed in PDFT, where fractional numbers of electrons in subsystems are treated using ensemble DFT.[22] Then the question becomes how to find this unique embedding potential in practice. In PDFT, Elliott *et al.* formulated the embedding potential (see Eq. (11) in Ref. 21) in the same way as in Cortona's original formalism (see Eq. (14) in Ref. 13). Both formulated the embedding potential in terms of density functionals, which makes different subsystems subject to different embedding potentials if the subsystem electron densities are not carefully chosen. Even though Elliott *et al.*[20,21] were able to impose the constraint that all subsystems share a common embedding potential, it was not straightforward to satisfy this constraint with their density-functional based formalism. Here we show that the key to imposing this constraint in a seamless way is to reformulate the total energy functional in terms of embedding potential functionals, instead of electron density functionals. In this framework, the embedding potential is used directly as the only working variable, and the total system's ground state is obtained by directly minimizing the total energy with respect to the embedding potential. During the minimization, the constraint is satisfied automatically and straightforwardly. As we show below, all four requirements enumerated above can be fulfilled simultaneously with our potential-functional formalism for the embedding theory. This potential-functional formalism is actually the dual problem to the density-functional formalism of the embedding theory.[20,21] In conventional

KS-DFT, this dual problem, i.e., the equivalence between density-based and potential-based total energy functionals, was already recognized some time ago.[23]

This paper is organized as follows. First, we introduce the potential-functional formalism for the embedding theory and prove that one has the freedom to choose any well-defined energy functional for describing subsystems. We then discuss use of either approximate kinetic energy density functionals (KEDFs) or optimized effective method (OEP) methods for evaluating the KS kinetic energy component of the interaction energy between subsystems. We then present how to efficiently calculate the gradient of the total energy with respect to the embedding potential and subsystem electron numbers. We also derive force expressions, so that geometry optimizations and dynamics will be possible. We then extend our theory to spin-polarized systems. To demonstrate our theory, we test it on several diatomic molecules, an H_6 chain, bulk NaCl, and the interaction between H_2O molecules and the MgO(100) surface.

II. THEORY

A. Potential-functional formalism for embedding theory

In every embedding theory, the total system is divided into two (or more) subsystems. A common way is to partition the total external ionic potential $V_{ext,total}(\vec{r})$ from all atoms into several subsystem potentials $V_{ext,K}(\vec{r})$ (where K indexes the subsystems),

$$V_{ext,total}(\vec{r}) = \sum_K V_{ext,K}(\vec{r}). \tag{1}$$

An embedding potential serves as an additional external potential to each subsystem, to replace the interaction between that subsystem and the rest of the total system. If we apply the constraint that all subsystems share one common embedding potential $u(\vec{r})$ and also fix the subsystem electron numbers $\{N_K\}$, we have shown[8] that this embedding potential $u(\vec{r})$ is unique. Once $u(\vec{r})$ and $\{N_K\}$ are known, the electron densities $\{\rho_K\}$ in the subsystems can be determined, as well as the total electron density $\rho_{tot} = \sum_K \rho_K$. Since ρ_{tot} uniquely determines the ground state of the total system due to the first HK theorem,[3] there is a one-to-one mapping between $u(\vec{r})$ and the total system with fixed $\{N_k\}$. Consequently, the problem of finding the ρ_{tot} that minimizes the total energy can be transformed to the problem of finding $u(\vec{r})$ and $\{N_K\}$ that minimize the total energy

$$\min_{\rho_{tot}} E_{tot}[\rho_{tot}] = \min_{u,\{N_K\}} E_{tot}[\rho_{tot}[u, \{N_K\}]], \tag{2}$$

which is the key idea in this work. The formal expression for the total energy functional E_{tot} in terms of $u(\vec{r})$ and $\{N_K\}$ is

$$E_{tot} = \sum_K E_K[u, N_K] + E_{int}[u, \{N_K\}]$$

$$+ \frac{1}{2} \sum_{I \in K} \sum_{J \in K' \neq K} \frac{Z_{I \in K} Z_{J \in K'}}{|\vec{R}_{I \in K} - \vec{R}_{J \in K'}|}. \tag{3}$$

The first term on the right-hand side is a sum over each subsystem's total energy functional in the presence of an

additional $u(\vec{r})$ for a given $\{N_K\}$. The ion-ion Coulomb interaction energies between different subsystems are grouped in the last term, with $\vec{R}_{I\in K}$ the coordinates and $Z_{I\in K}$ the full nuclear charge (for all-electron calculations) or the valence charge (for pseudopotential calculations) of nucleus I in subsystem K. $E_{\mathrm{int}}[u, \{N_K\}]$ is the interaction energy that will be discussed later. Note that Eq. (2) is equivalent to $\min_u \{\min_{\{N_K\}} E_{tot}[\rho_{tot}[u, \{N_K\}]]\}$, which means that $\{N_K\}$ is the minimizer for $E_{tot}[\rho_{tot}[u, \{N_K\}]]$ for a given $u(\vec{r})$. Throughout this work, we assume no degeneracies exist, i.e., there is only one unique $\{N_K\}$ for a given $u(\vec{r})$. This assumption is often satisfied in real physical systems, due to charge equilibration that produces an optimal set of $\{N_K\}$ for a given $u(\vec{r})$. Consequently, $\{N_K\}$ is an implicit functional of $u(\vec{r})$, which in turn renders E_{tot} a functional solely of $u(\vec{r})$. In this work, we demonstrate how to determine the embedding potential $u(\vec{r})$ and the subsystem electron numbers $\{N_K\}$.

B. Definition of the subsystem energy

Formally, a subsystem's energy functional is defined as

$$E_K[u, N_K, \{\vec{R}_{I\in K}\}] = E_{K0}[u, N_K, \{\vec{R}_{I\in K}\}]$$
$$+ \int \rho_K(\vec{r}) u(\vec{r}) dr^3, \qquad (4)$$

where $E_{K0}[u, N_K, \{\vec{R}_{I\in K}\}]$ is the total energy functional for the bare system K without embedding and where the embedding potential $u(\vec{r})$ serves as an external potential. Then we are free to evaluate E_K with, e.g., CW methods or other advanced quantum mechanics methods by treating $u(\vec{r})$ as an external potential.

In this work, for simplicity we use a KS-like definition for the subsystem energy E_{K0},

$$E_{K0} = -\sum_{i=occ} f_{K,i} \langle \phi_{K,i} | \frac{\nabla^2}{2} | \phi_{K,i} \rangle + J[\rho_K] + E_{xc}[\rho_K]$$
$$+ \int \rho_K(\vec{r}) V_{ext,K}(\vec{r}) dr^3$$
$$+ \frac{1}{2} \sum_{I\in K} \sum_{J\in K \text{ and } I\neq J} \frac{Z_{I\in K} Z_{J\in K}}{|\vec{R}_{I\in K} - \vec{R}_{J\in K}|}, \qquad (5)$$

where $f_{K,i}$ is the occupation number for the ith orbital in subsystem K, and $\sum_{i=occ} f_{K,i} = N_K$. $\{\phi_{K,i}\}$ are the KS orbitals in subsystem K, with $\sum_i f_{K,i} |\phi_{K,i}|^2 = \rho_K$. In contrast to the usual KS scheme, both N_K and $f_{K,i}$ are allowed to be fractional. $J[\rho_K]$ is the Hartree energy of the electron density in subsystem K. Here we use the local-density-approximation (LDA) (Ref. 24) for $E_{xc}[\rho_K]$ but of course one could also use more advanced XC functionals, such as orbital-dependent XC functionals.[5] The last two terms in Eq. (5) are the external potential energy (typically the ion-electron pseudopotential energy) and the ion-ion energy within subsystem K.

Our subsystem energy definition in Eq. (5) is different from PDFT,[18–21] where ensemble DFT is used to treat fractional electron numbers in subsystems. In ensemble DFT, the energy for a subsystem K with a fractional number $(N + \alpha)$ of

electrons is defined as[22]

$$E_K[N + \alpha] \equiv \alpha E_K[N] + (1 - \alpha) E_K[N + 1],$$

where $0 < \alpha < 1$ and $E_K[N]$ is the energy for an integer N electrons. One can argue that ensemble-DFT,[22] which is formulated for open systems, is physically correct for describing a fractional number of electrons. However, we can also employ other well-defined, convenient methods for subsystems because in the context of embedding theory only the total electron density ρ_{tot} enters the total energy functional E_{tot} (Eq. (2)). Consequently, one has the freedom to choose a different theory for each subsystem if it is desirable to do so. For example, if it was advantageous, one could use ensemble-DFT for some subsystems and use our definition (Eq. (5)) or CW methods for other subsystems. In the latter case, the electron numbers in those subsystems are required to be integers.

To verify whether the definition given in Eq (5) for the subsystem total energy E_K is well-defined, we need to show the one-to-one mapping between E_K and ρ_K. If there are an integer number of electrons in subsystem K, then this mapping is one-to-one due to the first HK theorem.[3] For subsystems having fractional numbers of electrons, the proof for the one-to-one mapping between E_K and ρ_K follows readily from the proof for the first HK theorem,[3] so we omit it here.

C. Definition of the interaction energy

The interaction energy E_{int} in Eq. (3) is defined to include *everything* that should be added to $\sum_K E_K$ and $\frac{1}{2} \sum_{I\in K} \sum_{J\in K' \neq K} Z_{I\in K} Z_{J\in K'}/|\vec{R}_{I\in K} - \vec{R}_{J\in K'}|$ in order to restore the total energy functional E_{tot}. Using the definition of the subsystem energy in Eq. (4), E_{int} is then

$$E_{\mathrm{int}} = E_{\mathrm{int}0} - \int u(\vec{r}) \rho_{tot} dr^3, \qquad (6)$$

where

$$E_{\mathrm{int}0} = \left(T_S[\rho_{tot}] - \sum_K T_S[\rho_K] \right)$$
$$+ \left(E_{xc}[\rho_{tot}] - \sum_K E_{xc}[\rho_K] \right) + J_{\mathrm{int}}[\{\rho_K\}]$$
$$+ \sum_K \int \rho_K(\vec{r}) \left(\sum_{K'\neq K} V_{ext,K'}(\vec{r}) \right) dr^3. \qquad (7)$$

Here, $T_S[\rho_K] = -\sum_{i=occ} f_{K,i} \langle \phi_{K,i} | \frac{\nabla^2}{2} | \phi_{K,i} \rangle$ and $T_S[\rho_{tot}]$ is the KS kinetic energy for the total density ρ_{tot}. J_{int} is defined as

$$J_{\mathrm{int}} = \sum_{K1} \sum_{K1\neq K2} \frac{1}{2} \iint \frac{\rho_{K1}(\vec{r}) \rho_{K2}(\vec{r}')}{|\vec{r} - \vec{r}'|} dr^3 dr'^3. \qquad (8)$$

It is easy to see that by inserting Eqs. (4)–(8) into Eq. (3), the total energy for the entire system is recovered,

$$E_{tot} = T_S[\rho_{tot}] + E_{xc}[\rho_{tot}] + J[\rho_{tot}] + \int V_{ext}(\vec{r}) \rho_{tot}(\vec{r}) dr^3$$
$$+ \frac{1}{2} \sum_I \sum_{J\neq I} \frac{Z_I Z_J}{|\vec{R}_I - \vec{R}_J|}, \qquad (9)$$

which only depends on the total electron density ρ_{tot} and the position of ions, as expected.

To evaluate E_{int}, XC functionals in Eq. (7) can be approximated with the LDA[24] or other advanced XC functionals.[5] To evaluate the KEDFs in Eq. (7), we can either calculate the exact kinetic energy and its potential for a given ρ_{tot} by employing the OEP method[25,26] or use approximate KEDFs. In this work, we use both the OEP method for the exact KEDF and some approximate KEDFs such as Thomas-Fermi (TF),[29] von Weizsäcker (vW),[30] and Huang-Carter[31] (HC10) KEDFs. For the HC10 KEDF, we set its two parameters to $\lambda = 0$ and $\beta = 0.65$, which is a simple nonlocal KEDF with a single-density dependent kernel appropriate for nearly-free-electron-like materials. The TF, vW, and HC10 ($\lambda = 0$) KEDFs allow us to test this potential-functional embedding theory with representative local, semilocal, and nonlocal KEDFs. In future work, we plan to examine other KEDFs such as the HC10 ($\lambda = 0.01$) that are appropriate for covalently bonded materials. In what follows, calculations with these approximate KEDFs are labeled as emb-OEP, emb-TF, emb-vW, and emb-HC10.

If we choose to use other methods than KS-DFT for some subsystems, e.g., CW or quantum Monte Carlo for subsystem A, then the interaction energy of Eq. (7) becomes

$$
\begin{aligned}
E_{int0} = & \left(T_S[\rho_{tot}] - \sum_{K \neq A} T_S[\rho_K] - T_S[\rho_A] \right) \\
& + \left(E_{xc}[\rho_{tot}] - \sum_{K \neq A} E_{xc}[\rho_K] - E_{XC}[\rho_A] \right) \\
& + J_{int}[\{\rho_K\}] + \sum_K \int \rho_K(\vec{r}) \left(\sum_{K' \neq K} V_{ext,K'}(\vec{r}) \right) dr^3.
\end{aligned}
$$
(10)

Here, we explicitly separate out the KS kinetic energy $T_S[\rho_A]$ and XC functional $E_{XC}[\rho_A]$ associated with the density ρ_A in subsystem A, where this density can be calculated from the many-body wavefunction. $T_S[\rho_A]$ can then be calculated by inverting the KS equations using the target density ρ_A, i.e., the OEP process,[25,26] and $E_{XC}[\rho_A]$ can then be calculated using whatever approximate XC functional is used for the other subsystems. This is directly analogous to how the embedding potential is formulated in earlier embedded CW schemes.[7,15,16] To embed CW calculations in DFT, Wesołowski[27] recently proposed a slightly different interaction energy, in which an additional term ΔF (see Eq. (29) in Ref. 27) is introduced, to treat the difference between the DFT total energy and the many-body total energy calculated based on correlated wave-function methods. However, when minimizing either the DFT (for degenerate quantum systems, we employ the Levy constrained search formulation[28]) or the correlated wave-function total energies, we search for all possible many-body wave-functions, and therefore the difference ΔF should be zero.
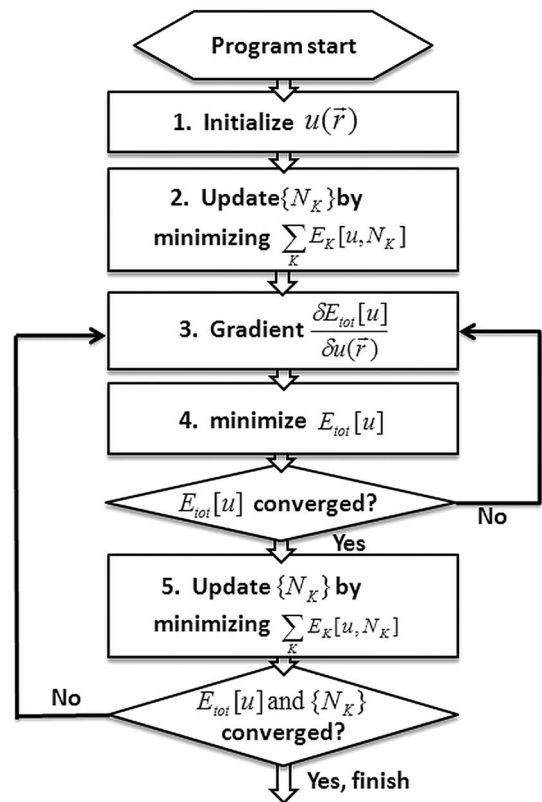

FIG. 1. Flow chart for total energy minimization with respect to the embedding potential $u(\vec{r})$ and subsystem electron densities $\{N_K\}$. After initializing $u(\vec{r})$, we solve for the subsystem electron numbers $\{N_K\}$ by minimizing $\sum_K E_K[u, N_K]$ with $u(\vec{r})$ fixed (step 2). In step 3, the gradient is calculated according to Eq. (20). With the gradient, we employ the quasi-Newton method (Ref. 40) to minimize $E_{tot}[u]$ (step 4). Once E_{tot} is minimized, we update $\{N_K\}$ with the new $u(\vec{r})$ (step 5). If E_{tot} and $\{N_K\}$ are both converged, the code exits, otherwise we go back to step 3.

D. Direct minimization of the total energy

Even though formally E_{tot} is a functional solely depending on the embedding potential $u(\vec{r})$, in practice E_{tot} is minimized in two separate steps. First, for a given $u(\vec{r})$, we minimize $\sum_K E_K$ with respect to $\{N_K\}$ with the constraint of conserving the total electron number $\sum_K N_K = N_{tot}$. Second, with fixed $\{N_K\}$, we minimize E_{tot} with respect to $u(\vec{r})$. We repeat these two steps until $u(\vec{r})$ and $\{N_K\}$ are both converged. A flow chart (Fig. 1) is given to illustrate the procedure.

We briefly discuss why this two-step procedure is valid for searching for the global minimum of E_{tot}. By minimizing E_{tot} with respect to $u(\vec{r})$ for a fixed $\{N_k\}$, we reach the condition

$$
\left. \frac{\delta E_{tot}}{\delta u(\vec{r})} \right|_{\{N_K\}} = 0,
$$

which is just the condition required for $u(\vec{r})$ at the global minimum of E_{tot}. Therefore the second step above is valid for searching the global minimum with respect to $u(\vec{r})$.

Now let's focus on $\{N_k\}$. By minimizing $\sum_K E_K$ with respect to $\{N_K\}$ for a given $u(\vec{r})$, we obtain the following equation:

$$
\left. \frac{\delta L}{\delta N_K} \right|_u = \left. \frac{\delta E_K}{\delta N_K} \right|_u - \mu = 0,
$$
(11)

where the Lagrangian is defined as $L = \sum_K E_K - \mu(\sum_K N_K - N_{tot})$.

In actuality, the equation that $\{N_K\}$ is required to satisfy at the global minimum of E_{tot} with fixed $u(\vec{r})$ is

$$\frac{\delta L_{tot}}{\delta N_K}\bigg|_u = \frac{\delta E_K}{\delta N_K}\bigg|_u + \frac{\delta E_{\text{int}}}{\delta N_K}\bigg|_u - \mu = 0, \qquad (12)$$

where the Lagrangian for the total system is defined as $L_{tot} = E_{tot} - \mu(\sum_K N_K - N_{tot})$. However, the term $\delta E_{\text{int}}/\delta N_K|_u$ in Eq. (12) is actually zero, as we now explain. Since the embedding potential $u(\vec{r})$ is defined as $u(\vec{r}) = \delta E_{\text{int0}}/\delta \rho_K(\vec{r})$[7,15,16] at the global minimum of E_{tot}, then we have

$$\frac{\delta E_{\text{int}}}{\delta N_K}\bigg|_u = \int \sum_K \frac{\delta\left(E_{\text{int0}} - \int u\rho_{tot}dr^3\right)}{\delta \rho_K(\vec{r})}\bigg|_u \frac{\delta \rho_K(\vec{r})}{\delta N_K}\bigg|_u dr^3$$

$$= \int \sum_K \left(\frac{\delta E_{\text{int0}}}{\delta \rho_K(\vec{r})}\bigg|_u - u(\vec{r})\right) \frac{\delta \rho_K(\vec{r})}{\delta N_K}\bigg|_u dr^3 = 0. \qquad (13)$$

Therefore Eq. (12) becomes

$$\frac{\delta L_{tot}}{\delta N_K}\bigg|_u = \frac{\delta E_K}{\delta N_K}\bigg|_u - \mu = 0.$$

Consequently, Eq. (11) that $\{N_K\}$ is required to satisfy at each optimization step is equivalent to Eq. (12) required for $\{N_k\}$ at the global minimum of E_{tot} with fixed $u(\vec{r})$. Hence, our two-step procedure for searching for the global minimum of E_{tot} is valid. Technical details of how to solve for $u(\vec{r})$ and $\{N_k\}$ are discussed in Subsections II F and II G below.

E. Uniqueness of the embedding potential

Under the assumption that there is only one set of $\{\rho_K\}$ for a given $u(\vec{r})$, it can be readily shown that the solution for the embedding potential $u(\vec{r})$ is unique up to a constant for a given quantum system, independent of any specific definitions for E_K and E_{int} discussed above. The detailed proof can be found in Cohen and Wasserman's work.[18] This assumption relies on two points. The first point is that for a given $u(\vec{r})$ only one set of $\{N_K\}$ exists, which was also assumed in Subsection II A and is usually satisfied due to charge equilibration that produces an optimal set of $\{N_K\}$. The second point is that, once $\{N_K\}$ is determined, the subsystems are assumed to obey the first HK theorem,[3] which implies that, for given N_K and $u(\vec{r})$ ($u(\vec{r})$ simply serves as an additional external potential), each subsystem is not degenerate and has only one ρ_K. In summary, going from a single quantum system to our embedding theory (containing multiple quantum subsystems), the original HK theorem[3] needs to be satisfied by each subsystem and the charge equilibration between subsystems is assumed to be unique.

F. Minimization of the total energy with respect to the embedding potential

To efficiently minimize E_{tot} with respect to $u(\vec{r})$ for a fixed $\{N_K\}$, we adapt the potential-based minimization tech-

nique of Gonze.[32] The gradient is formally

$$\frac{\delta E_{tot}}{\delta u(\vec{r})}\bigg|_{\{N_K\}} = \sum_K \frac{\delta E_K[u]}{\delta u(\vec{r})}\bigg|_{\{N_K\}} + \frac{\delta E_{\text{int}}[u]}{\delta u(\vec{r})}\bigg|_{\{N_K\}}. \qquad (14)$$

The first term on the right-hand side of Eq. (14) is

$$\frac{\delta E_K[u]}{\delta u(\vec{r})}\bigg|_{\{N_K\}} = \int \frac{\delta E_K[u]}{\delta \rho_K(\vec{r}')}\bigg|_u \frac{\delta \rho_K(\vec{r}')}{\delta u(\vec{r})}dr'^3 + \rho_K(\vec{r})$$

$$= \mu_K \int \frac{\delta \rho_K(\vec{r}')}{\delta u(\vec{r})}dr'^3 + \rho_K(\vec{r})$$

$$= \rho_K(\vec{r}). \qquad (15)$$

Here μ_K is the chemical potential for subsystem K, due to the constraint that the electron number in subsystem K is fixed. The integral in Eq. (15) is zero due to the conservation of the electron number under a small change in $u(\vec{r})$. According to Gonze's approach,[32] we have the identity

$$\frac{\delta \rho_K(\vec{r}')}{\delta u(\vec{r})} = \frac{\delta^2 E_K}{\delta u(\vec{r})\delta u(\vec{r}')} = \frac{\delta \rho_K(\vec{r})}{\delta u(\vec{r}')}. \qquad (16)$$

For the term $\delta E_{\text{int}}/\delta u(\vec{r})$ in Eq. (14), by the chain rule we have

$$\frac{\delta E_{\text{int}}}{\delta u(\vec{r})} = \sum_K \int \frac{\delta E_{\text{int}}}{\delta \rho_K(\vec{r}')} \frac{\delta \rho_K(\vec{r}')}{\delta u(\vec{r})}dr'^3. \qquad (17)$$

Inserting Eq. (16) into Eq. (17), we can use a first-order finite-difference expression to calculate the functional derivative

$$\frac{\delta E_{\text{int}}}{\delta u(\vec{r})} = \sum_K \int \frac{\delta E_{\text{int}}}{\delta \rho_K[u](\vec{r}')} \frac{\delta \rho_K[u](\vec{r})}{\delta u(\vec{r}')}dr'^3$$

$$\approx \sum_K \frac{1}{h_K} \left\{ \rho_K\left[u + h_K \frac{\delta E_{\text{int}}}{\delta \rho_K[u](\vec{r})}\bigg|_{u(r)}\right](\vec{r}) - \rho_K[u](\vec{r})\right\}. \qquad (18)$$

Here h_K is a small step used in the finite difference expression for each subsystem K. Eq. (18) can be calculated by performing another calculation for each subsystem K with a slightly different new embedding potential

$$u_K^{new} = u + h_K \frac{\delta E_{\text{int}}}{\delta \rho_K[u]}\bigg|_u.$$

As we approach the minimum, we find that a second order finite difference expression is necessary to obtain an accurate gradient

$$\frac{\delta E_{\text{int}}}{\delta u(\vec{r})} \approx \sum_K \frac{1}{2h_K} \left\{ \rho_K\left[u + h_K \frac{\delta E_{\text{int}}}{\delta \rho_K[u](\vec{r})}\bigg|_u\right](\vec{r}) - \rho_K\left[u - h_K \frac{\delta E_{\text{int}}}{\delta \rho_K[u](\vec{r})}\bigg|_u\right](\vec{r})\right\}. \qquad (19)$$

With the gradients (Eq. (14)) in hand, we can use routine optimization methods, such as conjugate gradient or quasi-Newton, to minimize E_{tot}.

G. Optimizing subsystem electron numbers

We give a general procedure to minimize $\sum_K E_K$ with respect to $\{N_K\}$ for a given embedding potential $u(\vec{r})$. To satisfy the constraint $\sum_K N_K = N_{tot}$, where N_{tot} is the number of electrons in the entire system, we employ the vector $\vec{x} = \{x_K\}$, instead of the original $\{N_K\}$, with $x_K^2 = N_K$ and $\sum_K x_K^2 = N_{tot}$. The Lagrangian then becomes a function of $\{x_K\}$,

$$L = \sum_K E_K[x_K] - \lambda \left(\sum_K x_K^2 - N_{tot} \right).$$

The Kth element of the steepest decent direction $\vec{d}$ is therefore

$$d_K = -\frac{\partial L}{\partial x_K} = -\left(\frac{\delta E_K}{\delta x_K} - 2\lambda x_K \right).$$

In the above, for a given $\vec{x}$ the Lagrange multiplier is taken to be

$$\lambda = \left(\sum_K \frac{dE[x_K]}{dx_K} x_K \right) \Big/ (2N_{tot}),$$

which will be exact at the minimum. We first determine the orthogonal projection of the vector $\vec{d}$ (perpendicular to $\vec{x}$),

$$\vec{d}_\perp = \vec{d} - \frac{\langle \vec{d} \mid \vec{x} \rangle \vec{x}}{|\vec{x}|^2},$$

where $\langle \vec{d} \mid \vec{x} \rangle$ is the inner product between vectors $\vec{d}$ and $\vec{x}$. Then $\vec{d}_\perp$ is normalized to be of length $\sqrt{N_{tot}}$,

$$\vec{d}_N = \vec{d}_\perp \frac{\sqrt{N_{tot}}}{\sqrt{\langle \vec{d}_\perp \mid \vec{d}_\perp \rangle}}.$$

The new $\vec{x}$ is then obtained by mixing the old $\vec{x}$ with the direction $\vec{d}_N$,

$$\vec{x}_{new} = \vec{x} \cos\theta + \vec{d}_N \sin\theta,$$

in which the mixing parameter θ is tuned from 0 to π to minimize $\sum_K E_K[x_K(\theta)]$. By using the variables $\{x_K\}$ instead of the original variables $\{N_K\}$, we always have $\sum_K x_{new,K}^2 = N_{tot}$ for any θ. And $x_K^2 = N_K$ guarantees that N_K is always positive.

To perform a line search for the optimal θ, we need to compute

$$\frac{d\left(\sum_K E_K[x_K(\theta)] \right)}{d\theta} = \sum_K \left(\frac{\delta E_K[x_{new,K}]}{\delta x_{new,K}} \frac{dx_{new,K}}{d\theta} \right)$$

$$= \sum_K \left(\frac{\delta E_K[x_{new,K}]}{\delta x_{new,K}} \right.$$

$$\left. \times (-x_K \sin\theta + d_{N,K} \cos\theta) \right).$$

Using the expressions above, we can efficiently optimize the electron numbers in subsystems.

In practice, we minimize the total energy with respect to $u(\vec{r})$ for a few steps with a fixed $\{N_K\}$, then we minimize $\sum_K E_K[x_K]$ with respect to $\{N_K\}$ with $u(\vec{r})$ being fixed, as shown in Fig. 1. To accelerate the convergence of electron numbers $\{N_K\}$, simple mixing or Anderson mixing,[33] often used for electron-density and potential mixing[34] in conventional KS-DFT calculations, can be employed.

H. Working with nonlocal pseudopotentials and entropy

Equation (3) is exact for local potentials, such as the $-Z/r$ potential for an ion with positive charge Z. To work with nonlocal pseudopotentials (NLPSs),[35,36] we need to modify the subsystem energy functional by adding the nonlocal terms. Working with the Kleinman-Bylander (KB) NLPSs,[36] the additional nonlocal electron-ion terms are centered at nuclei. Fortunately, these terms are short-ranged. Additionally, if a smearing technique is used in KS-DFT for efficient sampling of the Brillouin zone, we must include the associated entropy terms. We add two additional terms to Eq. (4) to obtain

$$E_K = E_{K0} + \int \rho_K u\, dr^3 + E_{NLPS}[\{\phi_{K,i}\}] - TS_K, \quad (20)$$

where $E_{NLPS}[\{\phi_{K,i}\}]$ is due to the use of KB-NLPSs and is defined as[36]

$$E_{NLPS}[\{\phi_{K,i}\}] = \sum_{i=occ} \sum_{\vec{R}} \sum_{l,m}$$

$$\times \frac{\langle \phi_{K,i} | \psi_{\vec{R},lm} \delta V_{\vec{R},lm} \rangle \langle \delta V_{\vec{R},lm} \psi_{\vec{R},lm} | \phi_{K,i} \rangle}{\langle \psi_{\vec{R},lm} | \delta V_{\vec{R},lm} | \psi_{\vec{R},lm} \rangle}.$$

$$(21)$$

Here, as in conventional KB-NLPSs, the $\psi_{\vec{R},lm}$ are the atomic pseudowavefunctions associated with the NLPS and $\delta V_{\vec{R},lm}$ are the lm angular momentum channels of the NLPS from which the local component has been subtracted, i.e., $V_{lm} - V_{loc}$.

Now, we discuss the range of the $\vec{R}$ summation in Eq. (21). If approximate KEDFs are used to evaluate the interaction energy E_{int0}, the sum over $\vec{R}$ in Eq. (21) will be over all the nuclei in the total system, rather than over just a single subsystem. This is because the wavefunctions in subsystem K interact with the KB-NLPS projectors from other subsystems, and therefore we have to include such interactions either in the subsystem energy functional (Eq. (5)) or in the interaction energy E_{int0} (Eq. (7)). Because direct functional derivatives $\delta E_{int0}/\delta \rho_K$ must be performed in the evaluation of Eq. (17), E_{int0} needs to be an explicit functional of electron density. Since the KB-NLPS energy functional $E_{NLPS}[\{\Phi_j[\rho_{tot}]\}]$ ($\{\Phi_j[\rho_{tot}]\}$ are the KS orbitals associated with the total electron density ρ_{tot} (the superposition of the subsystem electron densities) is not an explicit functional of electron densities, we cannot include $E_{NLPS}[\{\Phi_j[\rho_{tot}]\}]$ in E_{int0}. Thus, to consider the interaction between the NLPSs in one subsystem and the wavefunctions from other subsystems, we let $\vec{R}$ run over all atoms in the system in Eq. (21). However the situation changes if the OEP technique is used to evaluate E_{int0} directly. Via the OEP scheme, we have access to the functional derivative $(\delta T_S/\delta \rho_{tot} + \delta E_{NLPS}/\delta \rho_{tot})$ as a bundle. Consequently we can include $E_{NLPS}[\{\Phi_j[\rho_{tot}]\}]$ in the interaction energy E_{int0}, and we only need to include the

KB-NLPS projectors for atoms belonging to that subsystem in Eq. (21), i.e., $\vec{R}$ runs over the atoms only within each subsystem in Eq. (21). This in turn greatly simplifies the formalism with NLPSs and the derivation of forces later. However, throughout this work, to compare results using both KEDFs and OEP, we choose the case that $\vec{R}$ in Eq. (21) runs over all the atoms in the total system. Because of the short-range nature of the nonlocal terms of the pseudopotential, one could safely adopt a distance cutoff in future calculations involving KEDFs to limit the number of NLPS projectors included from neighboring subsystems.

When smearing is applied in KS-DFT, we need to consider an additional energy arising from the electronic entropy S_K in subsystem K, which is due to the statistics of Fermions with the Fermi-Dirac distribution,[37]

$$S_K = -k_B \int (f_K \ln f_K - (1 - f_K) \ln(1 - f_K)) N_K(\varepsilon) d\varepsilon,$$

where $N_K(\varepsilon)$ is the density of states in subsystem K, k_B is the Boltzmann constant, and f_K is the Fermi-Dirac distribution of occupation numbers over the non-interacting KS energy levels

$$f_K = \frac{1}{1 + e^{(\varepsilon_K - \mu_K)/k_B T}}.$$

T is the temperature.

Now let us focus on the interaction energy. The E_{int0} in Eq. (7) also needs to include E_{NLPS} and the energies due to the entropy

$$E_{int0}^{new} = E_{int0} + \left(E_{NLPS}[\{\Phi_j[\rho_{tot}]\}] - \sum_K E_{NLPS}[\{\phi_{K,i}\}] \right)$$
$$+ \left(-T S_{tot} + \sum_K T S_K \right), \tag{22}$$

where j loops over all occupied KS orbitals. S_{tot} is the entropy associated with the total system. Without the OEP, $\Phi_j[\rho_{tot}]$, $E_{NLPS}[\{\Phi_j[\rho_{tot}]\}]$, and S_{tot} cannot be evaluated and so we have to set the terms in the first parentheses and $-T S_{tot}$ to zero, i.e., $E_{int0}^{new} = E_{int0} + \sum_K T S_K$. For consistency, we also remove the subsystem entropy-related as well. For closed-shell molecules or materials with a moderate or large band gap, the entropy of the total system S_{tot} should be close to zero with a small smearing temperature anyway. In the non-OEP (the approximate KEDF) case, the interactions between the NLPSs in one subsystem and the wavefunctions from other subsystems are approximately treated via Eq. (21) by letting $\vec{R}$ run over all atoms in the system, as discussed above. With the OEP, $\Phi_j[\rho_{tot}]$, $E_{NLPS}[\{\Phi_j[\rho_{tot}]\}]$, and S_{tot} can be calculated for a given ρ_{tot}, therefore Eq. (22) can be fully evaluated, and the $\vec{R}$ in Eq. (21) runs over only the atoms in that subsystem.

I. First-order correction used in the Wu-Yang OEP

In some tests, we employ the Wu-Yang OEP[26] to evaluate the exact KS kinetic energy and its potential $(\delta T_S / \delta \rho(\vec{r}))$ for a given electron density ρ_0 (here a superposition of subsystem electron densities). After including NLPSs and entropy terms,

our modified Wu-Yang OEP is defined as

$$W[V_{eff}] = \left(-\sum_{i=occ} \langle \Phi_i | \frac{\nabla^2}{2} | \Phi_i \rangle + \int V_{eff}(\vec{r})(\rho(\vec{r}) \right.$$
$$\left. -\rho_0(\vec{r}))dr^3 - \int \eta |\nabla V_{eff}(\vec{r})|^2 dr^3 \right)$$
$$+ E_{NLPS}[\rho] + E_{TS}[\rho], \tag{23}$$

where the KS orbitals $\{\Phi_i\}$ are solved for each trial $V_{eff}(\vec{r})$, with $\rho(\vec{r}) = \sum_{i=occ} |\Phi_i|^2$. η is the penalty function coefficient. Therefore, W is a functional of $V_{eff}(\vec{r})$. The index i loops over all occupied orbitals. By maximizing $W[V_{eff}]$, we obtain the $V_{eff}(\vec{r})$ which reproduces the target electron density $\rho_0(\vec{r})$. The terms in parentheses are as defined in the original Wu-Yang OEP. Here the NLPS energy E_{NLPS} is only present if NLPSs are used and the entropy-related energy $E_{TS} = -T S_{tot}$. Since the basis set used for expanding the effective potential $V_{eff}(\vec{r})$ is frequently not balanced with respect to the basis set used for expanding the KS orbitals, a penalty function[38] (the last term in parentheses) is added to enforce the smoothness of $V_{eff}(\vec{r})$.

We find that use of a penalty function and other numerical inaccuracies cause the converged solution ρ_{opt} after maximizing Eq. (23) to be slightly different from the target electron density ρ_0. Therefore the kinetic energy calculated directly using $-\sum_{i=occ} \langle \Phi_i | \frac{\nabla^2}{2} | \Phi_i \rangle$ is not accurate. We show here that we can estimate the exact kinetic energy and its potential through a first-order correction. If NLPSs and smearing are used in KS-DFT calculations, the interaction energy (Eq. (22)) must also include the $E_{NLPS}[\rho_0]$ and $E_{TS}[\rho_0]$. Therefore what we are interested in is the sum of the $E_{NLPS}[\rho_0]$, $E_{TS}[\rho_0]$, and the kinetic energy all together. The exact sum of these three terms, estimated with a first-order correction, is

$$T_S[\rho_0] + E_{NLPS}[\rho_0] + E_{TS}[\rho_0]$$
$$= (T_S[\rho_{opt}] + E_{NLPS}[\rho_{opt}] + E_{TS}[\rho_{opt}])$$
$$+ \int \left. \frac{\delta (T_S + E_{NLPS} + E_{TS})}{\delta \rho(\vec{r})} \right|_{\rho_{opt}} (\rho_0 - \rho_{opt}) dr^3$$
$$= (T_S[\rho_{opt}] + E_{NLPS}[\rho_{opt}] + E_{TS}[\rho_{opt}])$$
$$+ \int (-V_{eff}[\rho_{opt}] + \mu[\rho_{opt}])(\rho_0 - \rho_{opt}) dr^3$$
$$= (T_S[\rho_{opt}] + E_{NLPS}[\rho_{opt}] + E_{TS}[\rho_{opt}])$$
$$+ \int V_{eff}[\rho_{opt}](\rho_{opt} - \rho_0) dr^3$$
$$= W[\rho_{opt}] + \int \eta |\nabla V_{eff}(\vec{r})|^2 dr^3. \tag{24}$$

In the above, the integral with the chemical potential is zero at convergence, due to the fact

$$\int \mu[\rho_{opt}](\rho_0 - \rho_{opt}) dr^3 = \mu[\rho_{opt}] (N_{tot} - N_{tot}) dr^3 = 0.$$

Therefore, after removing the penalty function, $W[\rho_{opt}]$ is just the first-order corrected $(T_S[\rho_{opt}] + E_{NLPS}[\rho_{opt}] + E_{TS}[\rho_{opt}])$ for $\rho_{opt} \to \rho_0$. Likewise, the first order correction to the potential of the sum of these three terms is given by

$$\frac{\delta (T_S + E_{NLPS} + E_{TS})}{\delta \rho(\vec{r})}\bigg|_{\rho_0} = -V_{eff}[\rho_{opt}] + \mu[\rho_{opt}]$$

$$+ \iint \frac{\delta^2 (T_S + E_{NLPS} + E_{TS})}{\delta \rho(\vec{r}')\delta \rho(\vec{r})}\bigg|_{\rho_{opt}}$$

$$\times (\rho_0 - \rho_{opt}) dr'^3. \quad (25)$$

In this work, we apply the first order correction from Eq. (24) to $(T_S[\rho_{opt}] + E_{NLPS}[\rho_{opt}] + E_{TS}[\rho_{opt}])$, which greatly improves the numerical accuracy of the OEP results. However, no correction for the potential is used, to avoid the calculation of the response function in the last integral in Eq. (25). We find that the method is stable without applying the correction to the potential.

J. Forces

Forces are required for modeling structural relaxation or dynamics. We show that it is straightforward to derive forces in this potential-functional embedding theory. Here we assume that $u(\vec{r})$ is expanded on a uniform grid (i.e., a plane-wave basis) independent of the nuclear coordinates.

In the following, we consider the case in which the OEP is used for the interaction energy term. Therefore each subsystem's energy functional only contains the KB-NLPSs of the atoms belonging to this subsystem. This greatly simplifies our force derivation below.

Forces are derived as

$$\vec{F} = -\frac{dE_{tot}[u[\{R_I\}], \{N_K[\{R_I\}]\}, \{R_I\}]}{d\vec{R}_{I\in A}}$$

$$= -\int \frac{\delta E_{tot}}{\delta u(\vec{r})}\bigg|_{\{N_K\},\{\vec{R}_I\}} \frac{\delta u(\vec{r})}{\delta \vec{R}_{I\in A}} dr^3$$

$$- \sum_K \frac{\delta E_{tot}}{\delta N_K}\bigg|_{u,\{\vec{R}_I\}} \frac{\delta N_K}{\delta \vec{R}_{I\in A}} - \frac{\partial E_{tot}}{\partial \vec{R}_{I\in A}}\bigg|_{\{N_K\},u}, \quad (26)$$

where $\vec{R}_{I\in A}$ are the coordinates for the atom I in subsystem A. Since $u(\vec{r})$ is the minimizer of E_{tot}, we have

$$\frac{\delta E_{tot}}{\delta u(r)}\bigg|_{\{N_K\}\{\vec{R}_I\}} = 0.$$

Because $\{N_K\}$ is the minimizer of E_{tot} with the constraint of conservation of total electron number, we have

$$\sum_K \left(\frac{\delta E_{tot}}{\delta N_K}\bigg|_{u,\{\vec{R}_I\}} \frac{\delta N_K}{\delta \vec{R}_{I\in A}}\right) = \sum_K \left(\mu \frac{\delta N_K}{\delta \vec{R}_{I\in A}}\right)$$

$$= \mu \sum_K \left(\frac{\delta N_K}{\delta \vec{R}_{I\in A}}\right) = 0,$$

where μ is the global chemical potential in the total system. Then only the last term in Eq. (26) remains. With the help of

Eq. (3), we have

$$\vec{F} = -\frac{\partial E_{tot}[u, \{\vec{R}_I\}]}{\partial \vec{R}_{I\in A}}\bigg|_{u,\{N_K\}}$$

$$= -\frac{\partial E_A}{\partial \vec{R}_{I\in A}}\bigg|_{u,N_A} - \frac{\partial E_{int}}{\partial \vec{R}_{I\in A}}\bigg|_{u,\{N_K\}}$$

$$- \frac{\partial}{\partial \vec{R}_{I\in A}} \left(\frac{1}{2}\sum_{I\in K}\sum_{J\in K'\neq K} \frac{Z_{I\in K}Z_{J\in K'}}{|\vec{R}_{I\in K} - \vec{R}_{J\in K'}|}\right)$$

$$= -\frac{\partial E_A}{\partial \vec{R}_{I\in A}}\bigg|_{u,N_A} - \frac{\partial E_{int}}{\partial \vec{R}_{I\in A}}\bigg|_{u,\{N_K\}}$$

$$- \frac{\partial}{\partial \vec{R}_{I\in A}} \left(\sum_{J\in K'\neq A} \frac{Z_{I\in A}Z_{J\in K'}}{|\vec{R}_{I\in A} - \vec{R}_{J\in K'}|}\right), \quad (27)$$

To obtain the last term on the last line above, we have used the fact that only subsystem A is affected by the change of $\vec{R}_{I\in A}$ for fixed $u(\vec{r})$ and $\{N_K\}$.

If subsystems are solved with a basis set that depends on $\{\vec{R}_I\}$, e.g., a Gaussian basis, then the subsystem electron densities $\{\rho_I\}$ explicitly depend on $\{\vec{R}_I\}$. In this case, we need to consider Pulay forces.[39] In Eq. (22), E_{NLPS} is an implicit functional of $\{\rho_I\}$, therefore E_{int} is a functional of $\{\rho_I\}$, $\{\vec{R}_I\}$, $\{N_K\}$, and $u(\vec{r})$. With $u(\vec{r})$ and $\{N_K\}$ fixed, the second term in Eq. (27) becomes

$$\frac{\partial E_{int}}{\partial \vec{R}_{I\in A}}\bigg|_{u,\{N_K\}} = \frac{\partial \left(E_{int0} - \int \rho_{tot} u dr^3\right)}{\partial \vec{R}_{I\in A}}\bigg|_{u,\{N_K\}}$$

$$= \left[\int \frac{\partial E_{int0}}{\partial \rho_A(\vec{r}')} \frac{\partial \rho_A(\vec{r}')}{\partial \vec{R}_{I\in A}} dr'^3 + \frac{\partial E_{int0}}{\partial \vec{R}_{I\in A}}\bigg|_{\{\rho_A\}} \right.$$

$$\left. - \int \frac{\partial \rho_{tot}}{\partial \vec{R}_{I\in A}} u(\vec{r}) dr^3 \right]_{u,\{N_K\}}. \quad (28)$$

In Eq. (28), we have separated the dependence of E_{int0} on $\vec{R}_{I\in A}$ into two parts: (1) the first term in the last line in Eq. (28) is due to the change of E_{int0} through the change of ρ_A with respect to $\vec{R}_{I\in A}$. Note that with fixed $u(\vec{r})$ and $\{N_K\}$, the change of $\vec{R}_{I\in A}$ only affects the density in subsystem A. (2) The middle term in the last line in Eq. (28) is due to the explicit coordinate dependence of E_{int0} on $\vec{R}_{I\in A}$ and the last term accounts for the implicit dependence of the total density on $\vec{R}_{I\in A}$.

We now show that the first and last terms in Eq. (28) cancel each other out. This is due to

$$\int \frac{\partial E_{int0}}{\partial \rho_A(\vec{r}')} \frac{\partial \rho_A(\vec{r}')}{\partial \vec{R}_{I\in A}} dr'^3 = \int u(\vec{r}') \frac{\partial \rho_A(\vec{r}')}{\partial \vec{R}_{I\in A}} dr'^3$$

$$= \int u(\vec{r}') \frac{\partial \rho_{tot}}{\partial \vec{R}_{I\in A}} dr'^3.$$

The remaining middle term in the last line in Eq. (28) is

$$\frac{\partial E_{int0}}{\partial \vec{R}_{I \in A}}\bigg|_{\{\rho_A\}} = \int \frac{dV_{Loc,A}}{d\vec{R}_{I \in A}} \left(\sum_K \rho_{K \neq A}\right) dr^3$$

$$+ \frac{\partial E_{NLPS}[\rho_{tot}, \{\vec{R}_I\}]}{\partial \vec{R}_{I \in A}}\bigg|_{\rho_{tot}}$$

$$- \frac{\partial E_{NLPS}[\rho_A, \{\vec{R}_I\}]}{\partial \vec{R}_{I \in A}}\bigg|_{\rho_A}$$

where $V_{Loc,A}$ would be the local part of the nonlocal pseudopotential of atom A.

Finally, the total force contains four parts:

$$\vec{F} = \vec{F}_0 + \vec{F}_1 + \vec{F}_{NLPS} + \vec{F}_2.$$

$\vec{F}_0$ is the first term in Eq. (27)

$$\vec{F}_0 = -\frac{\partial E_A}{\partial \vec{R}_{I \in A}}\bigg|_{u, N_A},$$

which are just the conventional forces in subsystem A, calculated in the presence of the embedding potential with fixed N_A.

$\vec{F}_1$ is the force between the nucleus I and the electron densities from the other subsystems, either due to the full nuclear charge electron-nuclear attraction or the local pseudopotential term

$$\vec{F}_1 = -\int \frac{dV_{Loc,A}}{d\vec{R}_{I \in A}} \left(\sum_{K \neq A} \rho_K\right) dr^3.$$

$\vec{F}_{NLPS}$ is the force due to the coordinate dependence of the NLPS projectors (centered at nuclei)

$$\vec{F}_{NLPS} = -\frac{\partial E_{NLPS}[\rho_{tot}, \{\vec{R}_I\}]}{\partial \vec{R}_{I \in A}}\bigg|_{\rho_{tot}}$$

$$+ \frac{\partial E_{NLPS}[\rho_A, \{\vec{R}_I\}]}{\partial \vec{R}_{I \in A}}\bigg|_{\rho_A}.$$

Finally, $\vec{F}_2$ is the electrostatic force between nucleus I and other nuclei outside subsystem A

$$\vec{F}_2 = -\frac{\partial}{\partial \vec{R}_{I \in A}} \left(\sum_{J \in K' \neq A} \frac{Z_{I \in A} Z_{J \in K'}}{|\vec{R}_{I \in A} - \vec{R}_{J \in K'}|}\right).$$

K. Spin-polarized systems

To extend our theory to magnetic cases, we modify the total energy expression in Eq. (3) in two ways to treat spin-polarized systems. One simple approach assumes that even if subsystems now contain different spin densities, the interactions between subsystems can still be described by one common scalar potential $u(\vec{r})$. Then the total energy is still the same as in Eq. (3); however, the interaction energy term (Eq. (7)) is modified to treat spins. For the collinear spin case,

we have

$$E_{int0} = \left(\frac{1}{2}T_S[2\rho_{tot,\uparrow}] + \frac{1}{2}T_S[2\rho_{tot,\downarrow}]\right)$$

$$- \sum_K \left(\frac{1}{2}T_S[2\rho_{K,\uparrow}] + \frac{1}{2}T_S[2\rho_{K,\downarrow}]\right)$$

$$+ \left(\frac{1}{2}E_{xc}[2\rho_{tot,\uparrow}] + \frac{1}{2}E_{xc}[2\rho_{tot,\downarrow}]\right)$$

$$- \sum_K \left(\frac{1}{2}E_{xc}[2\rho_{K,\uparrow}] + \frac{1}{2}E_{xc}[2\rho_{K,\downarrow}]\right)$$

$$+ J_{int} + \sum_K \int \rho_K(\vec{r}) \left(\sum_{K_2 \neq K} V_{K_2,ext}(\vec{r})\right) dr^3,$$

(29)

where the total electron density is $\rho_{tot} = \rho_{tot,\uparrow} + \rho_{tot,\downarrow}$ and subsystem electron densities are $\rho_K = \rho_{K,\uparrow} + \rho_{K,\downarrow}$.

More rigorously, magnetic subsystems should interact not only via a common scalar embedding potential $u(\vec{r})$ but also via an additional embedding magnetic field $B(\vec{r})$, as discussed in Ref. 8. In this case, the subsystem energy functional becomes

$$E_K = E_{K0} + \int \rho_K(\vec{r})u(\vec{r})dr^3 + \int [\rho_{K,\uparrow} - \rho_{K,\downarrow}]B(\vec{r})dr^3.$$

(30)

and the interaction energy term E_{int} becomes

$$E_{int} = E_{int,0} - \left(\int \rho_{tot}(\vec{r})u(\vec{r})dr^3\right.$$

$$\left. + \int [\rho_{tot,\uparrow} - \rho_{tot,\downarrow}]B(\vec{r})dr^3\right),$$

(31)

where $E_{int,0}$ is defined as in Eq. (29). It was shown in Ref. 8 that the partitioning of the spin-density (collinear case) and spin-density matrix (non-collinear case) is still unique for a common embedding potential $u(\vec{r})$ and embedding magnetic field $B(\vec{r})$ with fixed subsystem electron numbers. If subsystem electron numbers are allowed to vary, the previous proof for the non-spin-polarized case can be adapted to show the uniqueness of the partitioning of the spin-density or the spin-density matrix. Therefore minimization of the total energy functional still yields a unique solution for the spin-density or spin-density matrix partitioning. We leave the implementation of a spin-polarized embedding theory for future work.

III. NUMERICAL DETAILS

A FORTRAN90 code (named "UOPT") was written to perform this potential-functional embedding theory. As mentioned above, a flow chart of the code is given in Fig. 1. In UOPT, a quasi-Newton optimization code[40] is used to minimize the total energy with respect to the embedding potential $u(\vec{r})$. During the calculation, UOPT calls a modified ABINIT (Ref. 41) (named "mod-ABINIT") code with a trial $u(\vec{r})$ to perform standard KS-DFT calculations. This $u(\vec{r})$ serves as an additional external potential. Then mod-ABINIT returns with

a new ground state energy and electron density. If emb-OEP is performed, we have constructed another modified ABINIT code (named "inv-ABINIT") to find the corresponding KS kinetic energy and other quantities given an electron density, by performing the OEP algorithm discussed in both the Theory section and in Ref. 26. The penalty coefficient used in the OEP expression is small enough to ensure that the penalty function is smaller than 5×10^{-4} (atomic units). For H_2, P_2, Li-H, Na-H, K-H, bulk NaCl, and water/MgO(001) emb-OEP calculations, the penalty function coefficient is always 1×10^{-7}, and, for Al-P, the coefficient is 1×10^{-8}. We find that the final emb-OEP total energy is not sensitive to our small penalty functions. This is also due to the first order correction to the OEP total energy, as discussed in Subsection II I. All KS-DFT calculations in this work are done with the ABINIT code.[41] We note that for now our implementation can only treat nonmagnetic systems, so all calculations below are spin-restricted.

The LDA[24] XC functional is used for diatomic molecule tests (H_2, P_2, AlP, LiH, NaH, and KH) and the H_6 chain test. The generalized-gradient-approximation (GGA)[42] XC functional is used for bulk NaCl and the H_2O/MgO(001) tests. In the diatomic molecule tests, the equilibrium distances (relaxed using KS-DFT-LDA) between the two atoms in H_2, P_2, AlP, LiH, NaH, and KH are 0.7 Å, 2.0 Å, 2.2 Å, 1.8 Å, 1.8 Å, and 2.2 Å, respectively. For the H_6 setup, the distance between the nearest H atoms are 0.7 Å, and the chain is linear. In diatomic molecule tests, a cubic box with sides of 10 Å is used. In the H_6 chain test, the box is 17 Å×10 Å×10 Å to make sure the image interaction is very small.

We used both local and nonlocal pseudopotentials in a variety of tests of the theory. In the diatomic molecule and H_6 chain tests, we use local pseudopotentials (LPSs) in order to test the kinetic energy term in the interaction energy E_{int} and avoid NLPS terms in Eq. (22). To build an LPS for H, we first build its NLPS with the FHI98 code.[43] The LPS of H is then taken to be just the s angular momentum channel. We build LPSs for Li, Na, and K using the same procedure. For P and Al, we use bulk-derived LPSs[31,44] that we had already constructed for other purposes. For the NaCl and H_2O/MgO(001) tests, NLPSs are built with the FHI98 code. To achieve faster convergence of the total energy with respect to the number of plane waves (i.e., a small kinetic energy cutoff for the plane wave basis, E_{cut}), we build "soft" NLPSs for oxygen and hydrogen. For oxygen, the NLPS cutoff radii are 1.5, 2.0, and 2.0 bohr for the s, p, and d angular momentum channels. For hydrogen, the NLPS cutoff radius is 1.3 bohr for all s, p, and d angular momentum channels. We tested these soft NLPSs in a geometry relaxation of the water molecule using KS-DFT-GGA. The angle for H-O-H is 104.66 degrees, and the H-O bond is 0.946 Å, in good agreement with the target KS-DFT-GGA results, 104.33 degrees and 0.962 Å, obtained with NLPSs with the default cutoff radii in the FHI98 code.[43] In H_2, the H_6 chain, LiH, NaH, and KH tests, an E_{cut} of 1200 eV is employed to converge the total energy to within 10 meV. For P_2 and AlP diatomic molecules, the E_{cut} is 800 eV, since our Al and P BLPSs are set to zero at high frequency in Fourier space.[31]

In the bulk NaCl test, a cubic unit cell of four Na and four Cl atoms is employed. An E_{cut} of 1000 eV and a Monkhorst-Pack[45] k-point mesh of $2 \times 2 \times 2$ are used to converge the KS-DFT total energy to within 10 meV. To calculate the NaCl bulk modulus, Murnaghan's equation of state[46] is used. For the H_2O/MgO(001) test, a three-layer thick MgO(001) slab with a 1×1 periodic cell in the surface plane containing two Mg and two O atoms is used, with one water molecule added to one side of the slab (water coverage of 0.25 ML). A vacuum layer 12 Å thick is added above the MgO slab to limit interactions with periodic images. An E_{cut} of 1200 eV and a k-point mesh is $4 \times 4 \times 1$ converges the total energy to within 10 meV. The dipole interaction energy between slab periodic images in the surface normal direction is small, ~50 meV. The oxygen atom in the water molecule is fixed to be directly above one surface Mg atom, and the distance between them is varied. For each Mg-water O distance, only the H atoms are relaxed using ABINIT. These geometries are supplied to the following calculations and no further structure relaxations are performed. In all bulk and surface tests herein, Fermi-Dirac smearing with a smearing width of 0.1 eV is used to efficiently sample the Brillouin zone.

IV. RESULTS AND DISCUSSION

A. Diatomic molecules

We demonstrate our theory for several diatomic molecules (H_2, P_2, AlP, LiH, NaH, and KH) to consider both covalent and ionic bonding, as well as single and multiple bonds. In each test case, each atom is a subsystem. We start by considering the simplest case, H_2. In Fig. 2, the upper plot compares the emb-OEP, emb-vW, emb-TF, and emb-HC10 electron densities with the benchmark, which is a KS-DFT calculation on the entire H_2 molecule. We see a perfect match between emb-OEP and emb-vW densities with the benchmark. Since H_2 only contains two electrons, the vW KEDF is exact in this case. With emb-TF and emb-HC10, we see a deficiency of electron density between the two H atoms, which indicates that TF and HC10 KEDFs do not describe this covalent bond well. This disadvantage of the TF KEDF is manifest for the other diatomic molecules as well. Since TF theory is known not to bind atoms properly, it is not surprising that the TF KEDF is inadequate. However, the HC10 KEDF (with λ = 0) incorporates linear response behavior, which provides a superior description to emb-TF. In the lower plot of Fig. 2, we show a contour plot of the embedding potential from emb-OEP calculations. The embedding potential is zero far away from the H_2 molecule and is negative between H atoms to attract electrons to form bond.

P_2, with its 10 valence electrons and triple bond, provides a tougher test. In Fig. 3, the upper plot again compares the electron densities calculated with emb-OEP, emb-TF, and emb-HC10, against the benchmark obtained by performing restricted KS-DFT on the closed shell P_2 diatomic. In restricted KS-DFT, each KS orbital is occupied equally by spin up and spin down electrons. Because only the total electron density enters the total energy functional, our nonmagnetic treatment of each P atom (subsystem) is acceptable in systems
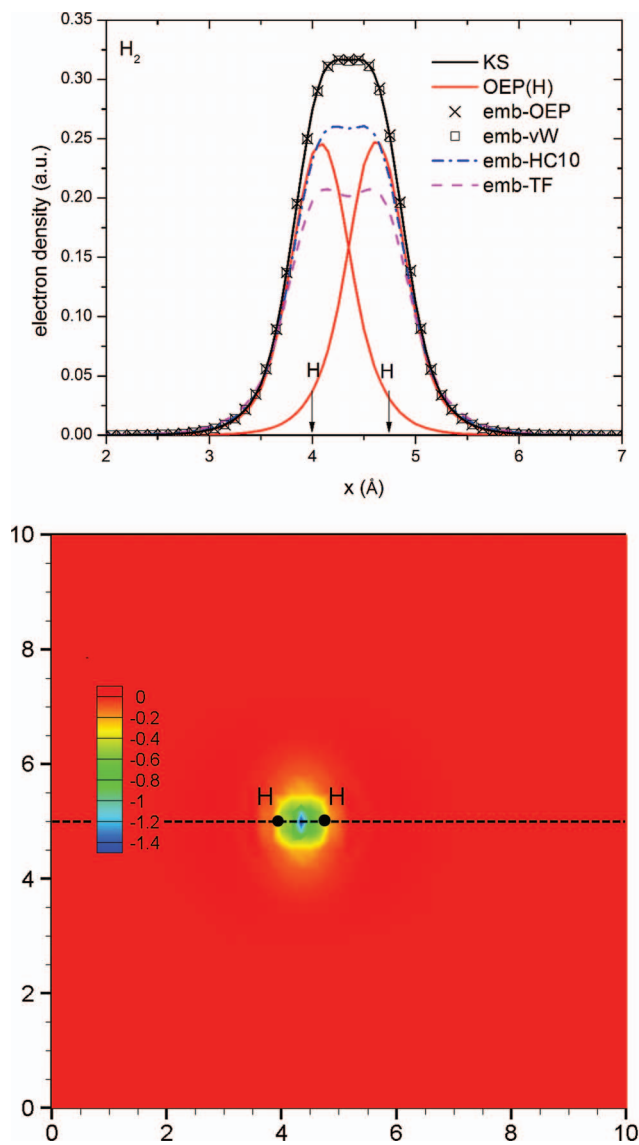
FIG. 2. (Upper plot) Comparison of electron densities along the H_2 molecular axis: KS-DFT density (benchmark) is the black curve. The emb-OEP, emb-vW, emb-HC10, and emb-TF densities are shown with black crosses, black open-squares, blue dash-dots, and pink dashes, respectively. The electron density of each H atom from the emb-OEP calculations is shown by the red solid curves. (Lower plot) Contour plot for the embedding potential (in Hartree $\cdot$ bohr^3) in a plane containing the H_2 molecule, with the coordinates in Å.

FIG. 3. (Upper plot) Comparison of electron densities along the P_2 molecular axis: KS-DFT density (benchmark) is the black curve. The emb-OEP, emb-HC10, and emb-TF results are given by the red circles, blue curve, and green curve, respectively. Electron densities for each P atom from the emb-OEP calculations are given by red solid curves. (Lower plot) Contour plot for the embedding potential (in Hartree $\cdot$ bohr^3) in a plane containing the P_2 molecule, with the coordinates in Å.

that are overall nonmagnetic. This is confirmed numerically for this P_2 case and all the following tests herein; we leave spin-polarized tests for future work. The emb-OEP (red circles) density matches the benchmark well, except at the middle peak where the emb-OEP density is slightly too high. This small mismatch is probably due to numerical inaccuracy in the OEP procedure. The emb-TF again gives too low an electron density in the bonding region (green curve), which indicates too weak covalent bonding. The emb-HC10 result (blue curve) overbinds slightly, with the density too high in the bonding region. The two red solid curves are the subsystem electron densities for the two P atoms respectively, which are localized around each P atom. The lower plot in Fig. 3 shows an embedding potential contour plot calculated with emb-
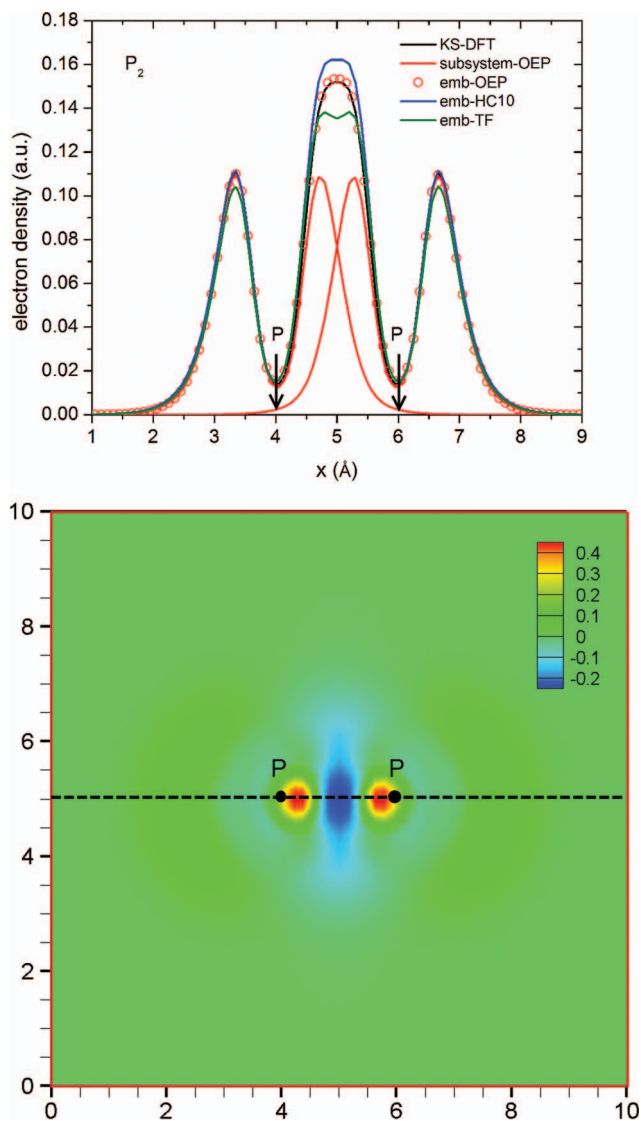
OEP. The red region is repulsive, which pushes electron densities to the negative blue region to form the covalent bond.

The above two homonuclear diatomic cases have no charge transfer between atoms due to symmetry. We now consider a polar covalent bond in the AlP diatomic. As in the P_2 case, the AlP molecule is treated as nonmagnetic within restricted KS-DFT. In Fig. 4, the upper plot again shows that the emb-OEP density (red circles) matches the benchmark (KS-DFT calculations on the AlP diatomic, solid black curve) very well. This time both emb-TF and emb-HC10 generate much too high electron density peaks around P atom. The middle plot of Fig. 4 shows the electron densities associated with each atom when emb-OEP is used. Again the subsystem electron densities are mainly localized at each atom and decays fast toward its neighbor. The contour plot in the lower plot of Fig. 4 shows a negative embedding potential (blue region) at
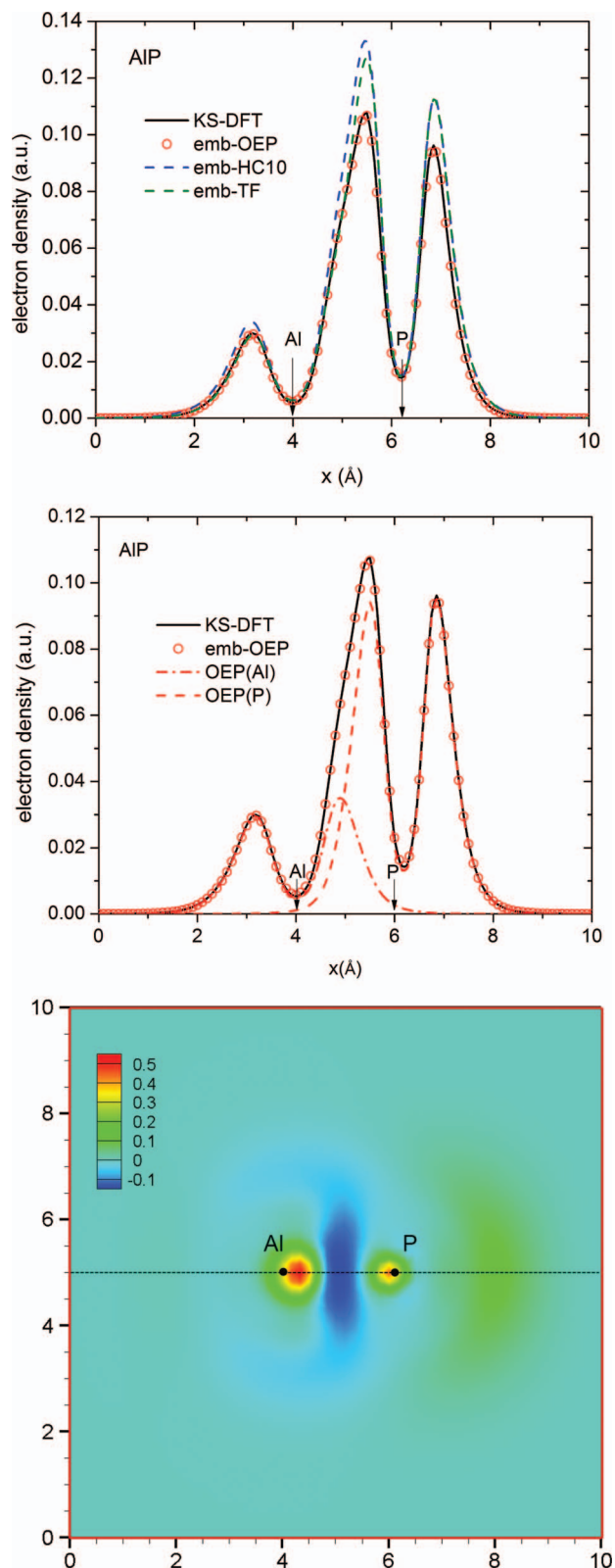
FIG. 4. (Upper plot) Comparison of electron densities along AlP bond axis: KS-DFT density (benchmark) is the black curve. The emb-OEP, emb-HC10, and emb-TF results are shown by red circles, blue dashes, and green dash-dots, respectively. (Middle plot) Electron densities of Al (red-dash dots) and P (red dashes) atoms from emb-OEP calculations. (Lower plot) Contour plot for the embedding potential (in Hartree · bohr^3) in a plane containing the AlP molecule, with the coordinates in Å.

TABLE I. Comparison of the total energies (eV) of the KS-DFT benchmark and the emb-OEP theory for H_2, P_2, AlP, LiH, NaH, and KH diatomic molecules.

	KS-DFT benchmark	Emb-OEP theory
H_2	− 30.862	− 30.860
P_2	− 359.701	− 359.698
AlP	− 233.533	− 233.525
LiH	− 20.445	− 20.443
NaH	− 19.658	− 19.659
KH	− 20.555	− 20.556

the bond and a repulsive embedding potential (red and yellow regions) near atoms. This shows that the character of the bond of AlP is not purely ionic but a polar-covalent bond. This polar-covalent bond is also confirmed in Table II, where the fractional electron number on Al atom is 2.63, close to three (the number of valence electrons for a neutral Al atom) but exhibiting a small amount of charge transfer to the P atom. In Table I, we give the total energies for H_2, P_2, and AlP calculated with both emb-OEP and the benchmark. Emb-OEP energies are consistently higher than the benchmarks, but only by at most 8 meV (for AlP).

To see how the embedding theory works for more ionic systems, we consider next three ionic diatomic metal hydride molecules LiH, NaH, and KH, where in each case only the two valence electrons are treated explicitly. In the upper plots of Fig. 5, Fig. 6, and Fig. 7, the emb-OEP densities (open-circles) match the KS-DFT benchmarks on the diatomics (black curves) very well. The contour plots of these embedding potentials (lower plots in Fig. 5, Fig. 6, and Fig. 7) show a clear trend of repulsive regions (red areas) moving successively towards the H atom from Li to K, which shows that K loses more electrons to the H atom, as expected from ionization energy trends. This trend is also seen in Table II, where the fractional electron numbers on metal atoms change from 0.42 to 0.28 from Li to K. In Table I, we compare the total energies between emb-OEP and the benchmark, where the energies differences are less than 2 meV for all three cases.

B. H_6 chain

We also performed emb-OEP on an H_6 chain as a first step toward treating many-atom systems, and compare the results against the benchmark obtained by performing KS-DFT on the whole H_6 chain (this example is similar to one used to demonstrate partition DFT in Ref. 20). Each H atom is a

TABLE II. Upper table: Fractional electron numbers on the metallic atoms (Al, Li, Na, and K) in the heteronuclear diatomic molecules studied here. Lower table: fractional electron numbers on H atoms from left to right (labeled from 1 to 6, see Fig. 8) in the H_6 chain. All results are from emb-OEP calculations.

Al-P	Li–H	Na–H	K–H		
2.63	0.42	0.43	0.28		

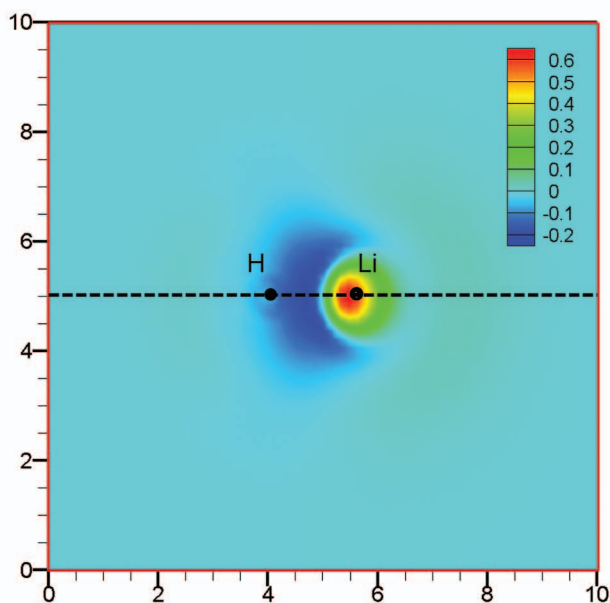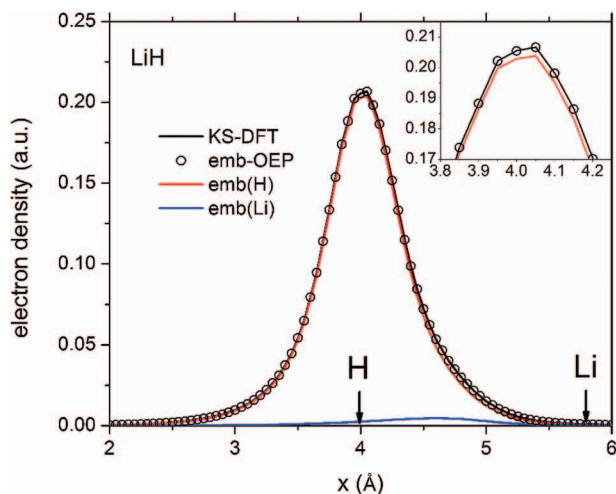| H_1	H_2	H_3	H_4	H_5	H_6
1.04	0.99	0.97	0.97	0.99	1.04

FIG. 5. (Upper plot) Comparison of electron densities along the LiH bond axis: KS-DFT density (benchmark) is given by the black curve and the emb-OEP density is shown in open circles. The inset shows the details at the peak of the density. Electron densities of H and Li atoms from emb-OEP calculations are shown by the red and blue curves. (Lower plot) Contour plot of the embedding potential (in Hartree·bohr^3) in a plane containing the diatomic molecule, with the coordinates in Å. The same convention is used in Figs. 6 and 7.

FIG. 6. (Upper plot) Comparison of electron densities along the NaH bond axis. (Lower plot) Contour plot of the embedding potential (in Hartree·bohr^3), with the coordinates in Å. See Fig. 5's caption for details.

subsystem. Fig. 8(a) displays a contour plot of the final embedding potential on a plane containing the H$_6$ chain. Negative regions of the embedding potential (green) are along the chain to attract electrons to form the bonds between H atoms. Surrounding the chain is a repulsive embedding potential (red and yellow regions) which further pushes electron density onto the chain. Fig. 8(b) shows a perfect match between the sum of electron densities from all subsystems (open circles) and the benchmark (black solid curve). Dashed curves show the electron densities associated with each H atom (subsystem). Again these densities are well localized at each atom. To further quantify how well our emb-OEP reproduces the benchmark, Fig. 8(c) displays a contour plot of the mismatch between the sum of all subsystem electron densities and the benchmark. A mismatch of $\sim 1 \times 10^{-3}$ a.u. is found around
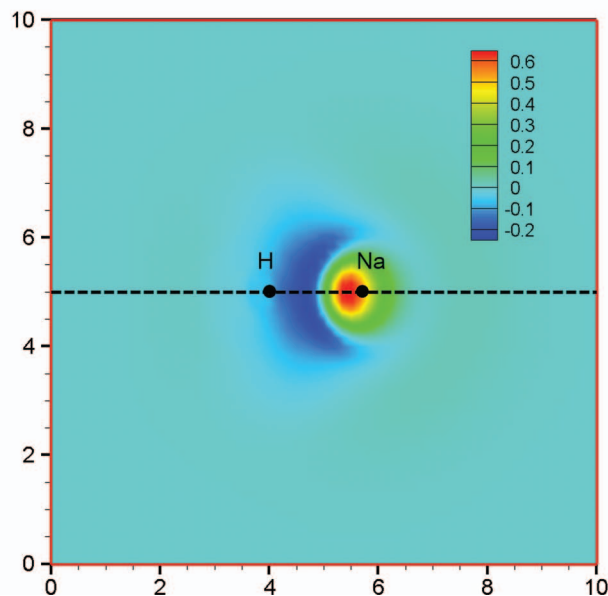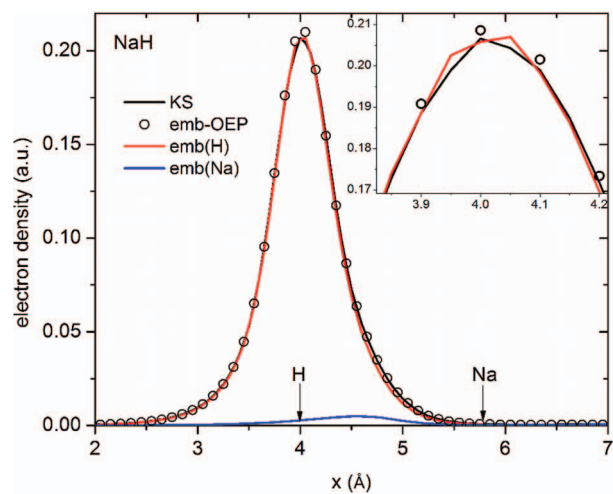
some H atoms. However the absolute value of electron density in these regions is $\sim 10^{-1}$ a.u. so the relative mismatch is quite small. The total energies of the benchmark and the emb-OEP differ by only 19 meV, a very small deviation. We conclude that our emb-OEP reproduces the benchmark very well.

The electron numbers on H atoms are shown in Table II. The H atoms at the two ends of the chain have the largest electron numbers (very slightly negatively charged). This result is consistent with the topology of the embedding potential (see Fig. 8(a)), in which the middle of the H chain is "squeezed" heavily by the positive embedding potential (the red region around the middle of the chain), and the two ends of the chain are surrounded by a negative ripple-like embedding potential.

C. NaCl bulk crystal

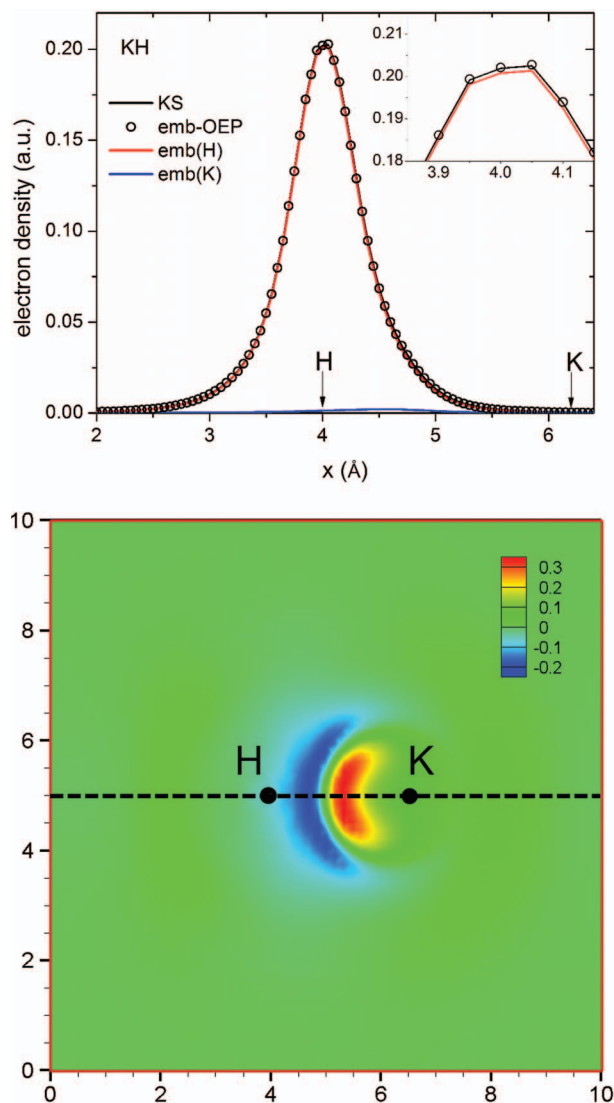We now test the potential-functional embedding theory in a periodic bulk crystal environment. Each atom in our cubic

FIG. 7. (Upper plot) Comparison of electron densities along the KH bond axis. (Lower plot) Contour plot of the embedding potential (in Hartree · bohr³), with the coordinates in Å. See Fig. 5's caption for details.
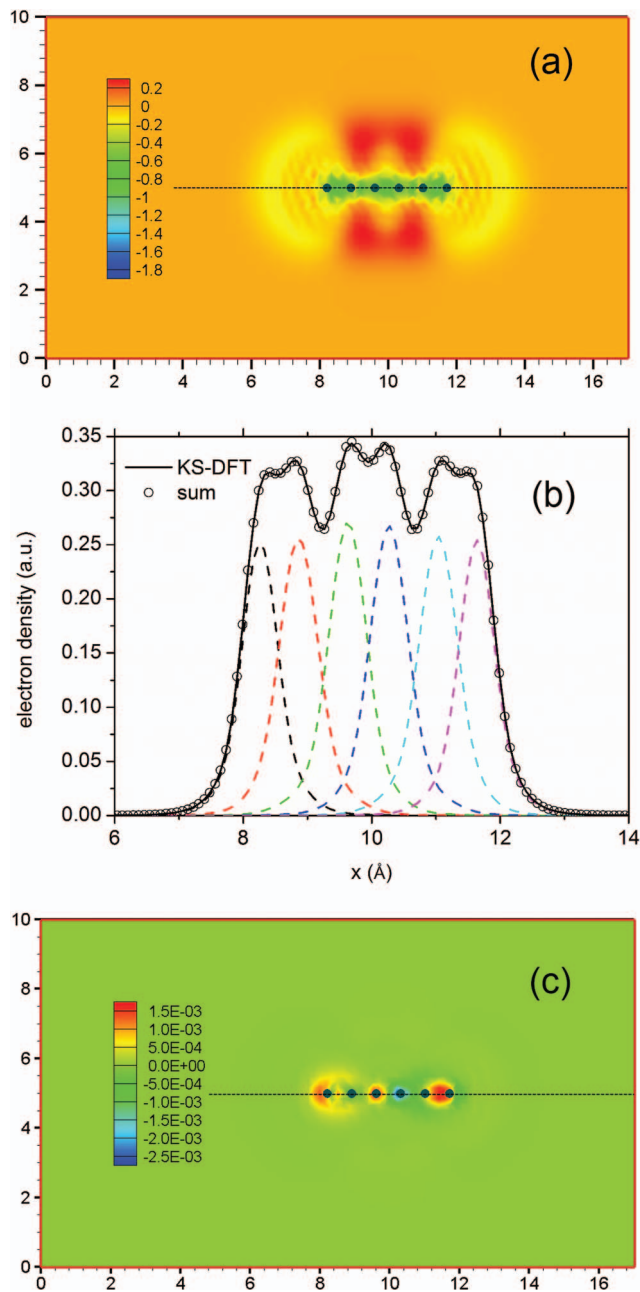

FIG. 8. (a) Contour plot of the embedding potential (Hartree · bohr³) from emb-OEP theory in a plane containing the H_6 chain, with coordinates in Å. The six hydrogen atoms are marked with black dots. (b) Comparison of the electron density along the H_6 chain for the KS-DFT benchmark (black solid curve) and the emb-OEP density sum (open circles). Subsystem electron densities are shown with dashes for each of the six hydrogen atoms. (c) Contour plot of the electron density difference between the KS-DFT benchmark and the emb-OEP scheme, with coordinates in Å.

unit cell of bulk NaCl (four Na and four Cl atoms) is treated as a subsystem and charge transfer is allowed. We perform both emb-TF and emb-OEP calculations. Since bulk NaCl is an ionic solid, the main cohesive energy is due to the electrostatic energy between ions. Therefore the short-range interaction energy due to partitioning of the KS kinetic energy and the XC energy should be small and we thus expect that emb-TF will describe NaCl reasonably well. This was also found in Cortona's calculation of bulk NaCl.[13] Our benchmark is a KS-DFT calculation on the NaCl unit cell. Fig. 9 shows the total energy per unit cell versus lattice constant, calculated with emb-OEP (crosses), emb-TF (triangles), and the benchmark (open squares). It is clear that emb-OEP agrees with the benchmark very well over a wide range of the lattice constant, while the emb-TF total energies are higher. However the shape of the emb-TF curve is very similar to the benchmark. The emb-TF curve deviates more strongly when the lattice constant goes beyond 6.4 Å, but this is already ∼10% larger than the equilibrium lattice constant (∼5.8 Å). A more de-

tailed comparison between the emb-OEP and the benchmark is presented in the inset of Fig. 9, where the differences between them are all <0.03 eV. We attribute this mismatch to numerical inaccuracies in the code and the use of a penalty function in the OEP process. The electron number of each Na atom changes almost linearly (from 0.001 to 0.003) with respect to the change of the lattice parameter. The tiny electron number on the Na atoms is consistent with the fact that Na atoms are almost fully ionized.
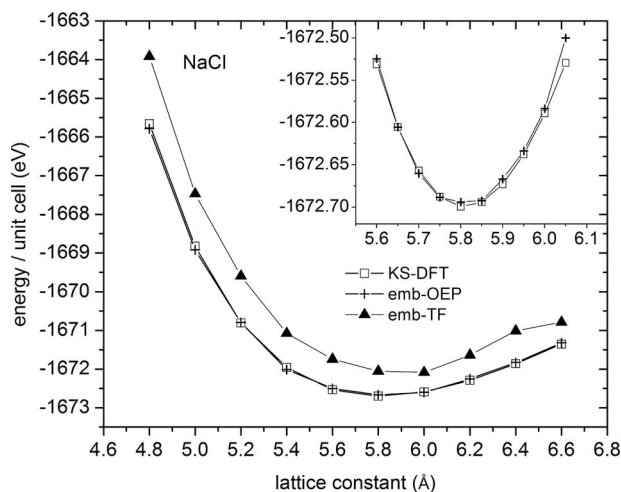
FIG. 9. Total energies (in eV) per cubic unit cell of bulk NaCl versus the lattice constant (in Å). The unit cell contains four Na and four Cl atoms. The KS-DFT results (the benchmark) are shown by open squares. The emb-TF (triangles) and emb-OEP (crosses) results are also shown. Inset: detailed comparison between the benchmark and emb-OEP results. The emb-OEP data almost coincide with the benchmark.

A more quantitative analysis of the emb-TF and emb-OEP results is given in Table III for the bulk modulus, equilibrium lattice constant, and equilibrium total energy per unit cell. The emb-OEP results agree with the KS-DFT results perfectly. The emb-TF results actually do not differ significantly from the KS-DFT, as also found in Cortona's theory given in Ref. 13.

D. H_2O on MgO(001)

Conventional KS-DFT employing LDA/GGA[8] or even a hybrid XC functional[47] often poorly describes molecular adsorption on surfaces. This is partially due to the fact that any charge transfer during bond formation between adsorbates and the surface requires an accurate calculation of eigenstates for both the surface and the adsorbate. However, conventional KS-DFT with approximate XC functionals often gives inaccurate eigenvalues, e.g., electron affinities and ionization energies. On the other hand, unphysical electron delocalization between adsorbate and surface can happen when LDA/GGA or even hybrid XC functionals are used, mainly due to (1) the incomplete cancellation of the self-interaction error[48] between the classical Hartree repulsion term and LDA/GGA/hybrid XC functionals, which in turn causes unphysical delocalization of electrons; (2) the lack of a derivative discontinuity[49] in LDA/GGA XC func-

TABLE III. Comparison of bulk NaCl bulk moduli (B_0 in GPa), equilibrium lattice constants (a_0 in Å), and equilibrium energy per unit cell (E_0 in eV) calculated via KS-DFT (the benchmark), emb-OEP theory, and emb-TF theory.

NaCl	B_0	a_0	E_0
KS-DFT benchmark	21	5.808	−1672.700
Emb-OEP theory	22	5.807	−1672.700
Emb-TF theory	19	5.898	−1672.063

tionals that makes charge transfer between an adsorbate and a surface subject to no barrier even when they are far away from each other.[49] In the next example, we demonstrate our potential-functional embedding theory, which provides a self-consistent framework to tackle such surface-related problems. To demonstrate how our self-consistent potential-functional embedding theory performs, it is sufficient to only show DFT-in-DFT embedding calculations here. To describe adsorption more accurately will require treating the region of interest with potential functional embedded CW methods, which represents the next stage in our research.

We study the interaction between a water molecule and the MgO(001) surface. Fig. 10 shows the total energy versus the distance between the O atom in the H_2O molecule and the MgO surface. The benchmark is calculated by performing KS-DFT-GGA on the entire H_2O/MgO(001) system. The "shift-bare-ML" results (blue triangles) are calculated by performing KS-DFT-GGA on the water molecule and the first layer of the MgO surface, with the resulting energies then shifted downward by 1819.879 eV to match the benchmark at $d = 4.0$ Å. The shift-bare-ML results are consistently lower than the benchmark by 20 meV or less after shifting. The embedding results are obtained by treating the water molecule and the first periodically replicated layer of MgO as one subsystem, with the other two periodically replicated layers of MgO as another subsystem. Each subsystem is treated using KS-DFT-GGA. For simplicity, we did not optimize subsystem electron numbers, and each subsystem is kept neutral. This is a physical choice, since we do not observe a large charge transfer between the water molecule and the MgO surface in our benchmark calculations. The emb-TF curve is shifted downward, by only 2.539 eV (labeled "shift-emb-TF," green circles) to match the benchmark at $d = 4.0$ Å. The "shift-emb-TF" results are closer to the benchmark than "shift-bare-ML," which is consistent with the fact that for ionic systems near equilibrium, such as bulk NaCl demonstrated above, the TF
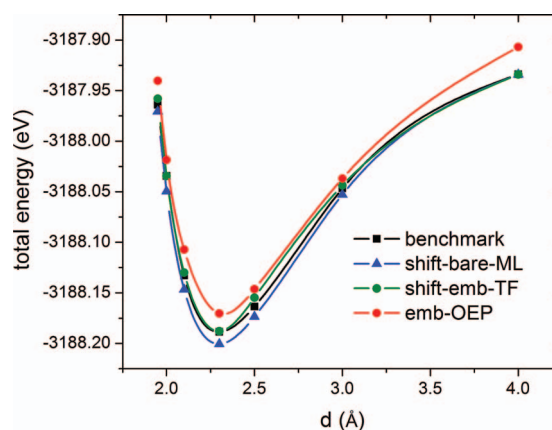

FIG. 10. Total energy versus the distance d between the water molecule and the MgO(001) surface. Comparison between the benchmark (black squares), non-embedded results (labeled "shift-bare-ML," blue triangles), shifted emb-TF results (labeled "shift-emb-TF," green circles), and emb-OEP results (red circles). Both shift-bare-ML (shifted downwards by 1819.879 eV) and shift-emb-TF (shifted downwards by 2.539 eV) data are shifted to match the benchmark at $d = 4.0$ Å. The emb-OEP results are not shifted and are consistently higher than the benchmark, but with a small absolute error of less than 30 meV.
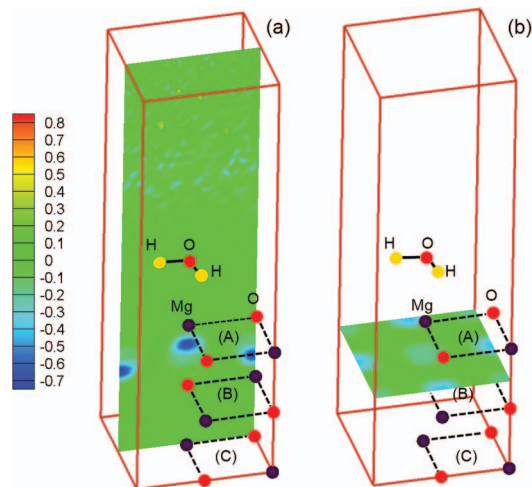
FIG. 11. Two contour plots of the embedding potential (in Hartree·bohr^3) for the H_2O molecule 2.3 Å above the MgO (100) surface. The O atom in the water molecule is directly above the labeled Mg atom in plane (A). Due to the periodicity, we only show the Mg and O atoms in the unit cell. The upper part of the cell is vacuum. The boxes with red edges are the unit cells used in our calculations. O, H, and Mg atoms are shown in red, yellow, and purple, respectively. (a) The contour plot is on the plane cut through the labeled Mg and O atoms, and is perpendicular to the MgO surface. (b) The contour plot is on a plane bisecting the top two layers (A) and (B), and is parallel to the MgO surface.

KEDF is a reasonable choice. For the emb-OEP results (red circles), the total energies are already very close to the benchmark so no shift is necessary. The emb-OEP results are consistently higher than the benchmark, but only by ∼30 meV.

Figure 11 displays a contour plot of the embedding potential from emb-OEP calculations. The plot is drawn at the H_2O-Mg distance of 2.3 Å (the energy minimum in Fig. 10). We see small ripples in the vacuum region (above the water molecule), probably due to numerical noise. It is clear that the embedding potential decays very fast away from the surface monolayer, and is almost zero between layer (B) and layer (C). In Figs. 11(a) and 11(b), the positive embedding potential (repulsive) is around Mg atoms to push electrons to O atoms, where the negative embedding potential (attractive) is located.

V. CONCLUSIONS

In this work, we have introduced a potential-functional embedding theory. The total energy is formulated as a functional of the embedding potential. In contrast to previous work[13,20,21] in which the basic working variables are electron densities (density-functional based), in our approach the embedding potential is used directly as the only working variable. Consequently, it is straightforward to impose the constraint that all subsystems share a common embedding potential. In conventional KS-DFT, it was already recognized that the potential-functional based formalism is dual to the density-functional based formalism.[23] In this work, we have extended this dual relationship to potential-functional embedding theory. We have shown that the ground state of the total system can be solved with an unconstrained minimization of the total energy with respect to the embedding potential. Therefore our theory can be implemented using efficient

optimization algorithms and it is straightforward to satisfy the constraint that all subsystems share a common embedding potential. We also derived expressions for forces on nuclei, for future simulations in which structural relaxation and dynamics are envisioned. We have shown that it is valid to choose different methods for describing different subsystems, since it is the total electron density that finally enters the total energy functional. This finding provides the theoretical foundation for using CW methods or any other advanced quantum mechanics methods in the density-based embedding theory.

In order to solve for the embedding potential efficiently, we derive the gradient of the total energy with respect to the embedding potential. A two-step optimization procedure to minimize the total energy is introduced. We discussed in detail how to implement our theory with nonlocal pseudopotentials (NLPSs) and entropy contributions arising from Fermi surface smearing techniques for sampling the Brillouin zone. We extended the formal theory to spin-polarized quantum systems so as to make it applicable to magnetic materials and open-shell molecules in the future.[50]

To demonstrate the accuracy of our new embedding theory, we tested it on several diatomic molecules: H_2, P_2, AlP, LiH, NaH, and KH, and a chain of H atoms. When an OEP scheme is used to evaluate the kinetic energy terms (associated with the total electron density) in the interaction energy E_{int}, the embedding results agree with the benchmarks very well. We also tested the theory on bulk NaCl and an adsorbate-surface interaction, namely water on MgO. In all these tests, we find that the emb-OEP theory is in excellent agreement with KS-DFT calculations done on the entire system.

The potential-functional embedding theory presented in this work is a unified framework for interconnecting different subsystems treated with different levels of quantum mechanics methods in a seamless way. Here we only performed DFT-in-DFT calculations with LDA and GGA XC functionals to demonstrate the approach, but in practice, any first-principles method that delivers ground state electron densities and total energies can be used to achieve an accurate description for the subsystem of interest. Such methods include KS-DFT equipped with advanced orbital-based XC functionals, *ab initio* correlated wavefunction theories, quantum Monte Carlo methods, etc. With the ground state electron densities obtained from these methods, the OEP scheme can be used to find the related orbital-based KS-DFT quantities, i.e., the KS kinetic energy, the NLPS energy, energies due to the electronic entropy (if smearing is used), which are needed for our embedding theory. If the OEP scheme is employed, the accuracy of the embedding potential is then only determined by the choice of approximate XC functional used in the interaction energy.

Regarding computational cost, the most time consuming steps are steps 2 and 3 in the flow chart (Fig. 1). In these two steps, we perform expensive calculations on subsystems. Therefore it is preferable to divide the total system into subsystems that are as small as possible, especially for those subsystems to which highly-accurate quantum mechanics methods are applied. Each subsystem could be treated independently via parallel processing. In step 2 of Fig. 1, the

number of iterations needed to minimize $\sum_K E_K[u, N_K]$ with respect to $\{N_K\}$ is unknown. Therefore, if the electron numbers in subsystems can be determined beforehand through some physical intuition, we recommend fixing electron numbers in subsystems. In the $H_2O/MgO(001)$ test, within about ten iterations the total energies converge to within 1 mHa using a quasi-Newton optimization code.[40] However, we did not optimize the subsystem electron numbers in this case, which greatly reduced the computational cost. To compute $\delta E / \delta u$ in step 3 of Fig. 1, all subsystems are calculated twice when using the first-order finite difference (see Eq. (18)) or three times when using the second-order finite difference (see Eq. (19)) expression, during each pass of the flow chart. In step 3, if the OEP scheme is used for computing the KS kinetic energy and potential in Eq. (22), the computational cost for inverting the KS equations for a given total electron density will be comparable to an ordinary KS-DFT calculation on the entire system. This invert-KS procedure is performed every time during each pass of the flow chart. Once we approach the minimum of the total energy $E_{tot}[u]$, the convergence of this invert-KS procedure is much faster, since the output from the previous run is a good initial guess for the current run.

As a last point, we believe our potential-functional embedding theory will be useful for tackling those difficult problems in material science and perhaps biochemistry, where highly accurate *ab initio* methods are required for a particular region of interest (e.g., an active site in an enzyme) in order to have a reliable understanding of properties of matter. If made computationally efficient, it could provide the means to treat large covalently bonded molecules such as proteins in a seamless embedding framework.

ACKNOWLEDGMENTS

[1] M. Schütz, R. Lindh, and H. J. Werner, Mol. Phys. **96**, 719 (1999); M. Schütz, G. Hetzer, and H. J. Werner, J. Chem. Phys. **111**, 5691 (1999); M. Schütz and H. J. Werner, J. Chem. Phys. **114**, 661 (2001); N. Flocke and R. J. Bartlett, J. Chem. Phys. **121**, 10935 (2004); T. S. Chwee, A. B. Szilva, R. Lindh, and E. A. Carter, J. Chem. Phys. **128**, 224106 (2008).

[2] W. Kohn and L. J. Sham, Phys. Rev. **140**, A1133 (1965).

[3] P. Hohenberg and W. Kohn, Phys. Rev. **136**, B864 (1964).

[4] J. P. Perdew and K. Schmidt, AIP Conf. Proc. **577**, 1 (2001); A. E. Mattsson, Science **298**, 759 (2002).

[5] S. Kümmel and L. Kronik, Rev. Mod. Phys. **80**, 3 (2008).

[6] W. Kohn, Phys. Rev. Lett. **76**, 3168 (1996); E. Prodan and W. Kohn, Proc. Natl. Acad. Soc. U.S.A. **76**, 3168 (2005).

[7] S. Sharifzadeh, P. Huang, and E. A. Carter, J. Phys. Chem. C **112**, 4649 (2008).

[8] C. Huang, M. Pavone, and E. A. Carter, J. Chem. Phys. **134**, 154110 (2011).

[9] B. G. Dick and A. W. Overhauser, Phys. Rev. **112**. 603 (1958); P. V. Sushko, A. L. Shluger, and C. R. A. Catlow, Surf. Sci. **450**, 153 (2000).

[10] L. Seijo and Z. Barandiarán, *Computational Chemistry: Reviews of Current Trends*, Vol. 4, edited by J. Leszczynski (Wold Scientific, Singapore, 1999), pp. 55–152.

[11] A. Redondo, W. A. Goddard III, C. A. Swarts, and T. C. McGill, J. Vac. Sci. Technol. **19**, 498 (1981).

[12] G. Senatore and K. R. Subbaswamy, Phys. Rev. B **34**, 5754 (1986).

[13] P. Cortona, Phys. Rev. B **44**, 8454 (1991).

[14] T. A. Wesolowski and A. Warshel, J. Phys. Chem. **97**, 8050 (1993); **98**, 5183 (1994); T. A. Wesolowski and J. Weber, Chem. Phys. Lett. **248**, 71 (1996).

[15] N. Govind, Y. A. Wang, A. J. R. da Silva, and E. A. Carter, Chem. Phys. Lett. **295**, 129 (1998); N. Govind, Y. A. Wang, and E. A. Carter, J. Chem. Phys. **110**, 7677 (1999); T. Klüner, N. Govind, Y. A. Wang, and E. A. Carter, Phys. Rev. Lett. **86**, 5954 (2001); T. Klüner, N. Govind, Y. A. Wang, and E. A. Carter, *ibid.* **88**, 209702 (2002); T. Klüner, N. Govind, Y. A. Wang, and E. A. Carter, J. Chem. Phys. **116**, 42 (2002).

[16] P. Huang and E. A. Carter, J. Chem. Phys. **125**, 084102 (2006); S. Sharifzadeh, P. Huang, and E. A. Carter, Chem. Phys. Lett. **470**, 347 (2009).

[17] P. Huang and E. A. Carter, Annu. Rev. Phys. Chem. **59**, 261 (2008).

[18] M. H. Cohen and A. Wassermann, J. Stat. Phys. **125**, 1125 (2006).

[19] M. H. Cohen and A. Wasserman, Israel J. Chem. **43**, 219 (2003); M. H. Cohen and A. Wasserman, J. Phys. Chem. A **111**, 2229 (2007).

[20] P. Elliott, K. Burke, M. H. Cohen, and A. Wasserman, Phys. Rev. A **82**, 024501 (2010).

[21] P. Elliott, M. H. Cohen, A. Wasserman, and K. Burke, J. Chem. Theory Comput. **5**, 827 (2009).

[22] J. P. Perdew, R. G. Parr, M. Levy, and J. L. Balduz, Jr., Phys. Rev. Lett. **49**, 1691 (1982).

[23] W. Yang, P. W. Ayers, and Q. Wu, Phys. Rev. Lett. **92**, 146404 (2004).

[24] J. P. Perdew and Y. Wang, Phys. Rev. B **45**, 13244 (1992).

[25] Y. Wang and R. G. Parr, Phys. Rev. A **47**, R1591 (1993); R. van Leeuwen and E. J. Baerends, Phys. Rev. A **49**, 2421 (1994); Q. S. Zhao, R. C. Morrison, and R. G. Parr, Phys. Rev. A **50**, 2138 (1994); R. A. King and N. C. Handy, Phys. Chem. Chem. Phys. **2**, 5049 (2000); O. Roncero, M. P. de Lara-Castells, P. Villarreal, F. Flores, J. Ortega, M. Paniagua, and A. Aguado, J. Chem. Phys. **129**, 184104 (2008); O. Roncero, A. Zanchet, P. Villarreal, and A. Aguado, *ibid.* **131**, 234110 (2009).

[26] Q. Wu and W. Yang, J. Chem. Phys. **118**, 2498 (2003).

[27] T. A. Wesołowsk, Phys. Rev. A **77**, 012504 (2008).

[28] M. Levy, Proc. Natl. Acad. Sci. USA **76**, 6062 (1979); M. Levy, Phys. Rev. A. **26**, 1200 (1982).

[29] L. H. Thomas, Proc. Cambridge Philos. Soc. **23**, 542 (1927); E. Fermi, Rend. Accad. Naz. Lincei **6**, 602 (1927); E. Fermi, Z. Phys. **48**, 73 (1928).

[30] C. F. v. Weizsäcker, Z. Phys. **96**, 431 (1935).

[31] C. Huang and E. A. Carter, Phys. Rev. B **81**, 045206 (2010).

[32] X. Gonze, Phys. Rev. B **54**, 4383 (1996).

[33] D. G. Anderson, J. Assoc. Comput. Mach. **12**, 547 (1965).

[34] P. H. Dederichs and R. Zeller, Phys. Rev. B **28**, 5462–5472 (1983).

[35] D. R. Hamann, M. Schlüter, and C. Chiang, Phys. Rev. Lett. **43**, 1494 (1979).

[36] L. Kleinman and D. M. Bylander, Phys. Rev. Lett. **48**, 1425 (1982).

[37] G. Grimvall, *Thermophysical Properties of Materials* (North-Holland, Amsterdam, 1986).

[38] T. Heaton-Burgess, F. A. Bulat, and W. Yang, Phys. Rev. Lett. **98**, 256401 (2007).

[39] P. Pulay, Mol. Phys. **17**, 197 (1969).

[40] R. H. Byrd, P. Lu, J. Nocedal, and C. Zhu, SIAM J. Sci. Comput. **16**, 1190 (1995).

[41] X. Gonze, B. Amadon, P. Anglade, J.-M. Beuken, F. Bottin, P. Boulanger, F. Bruneval, D. Caliste, R. Caracas, M. Côté, T. Deutsch, L. Genovese, P. Ghosez, M. Giantomassi, S. Goedecker, D. Hamann, P. Hermet, F. Jollet, G. Jomard, S. Leroux, M. Mancini, S. Mazevet, M. Oliveira, G. Onida, Y. Pouillon, T. Rangel, G.-M. Rignanese, D. Sangalli, R. Shaltaf, M. Torrent, M. Verstraete, G. Zerah, and J. Zwanziger, Comput. Phys. Commun. **180**, 2582 (2009).

[42] J. P. Perdew, K. Burke, and M. Ernzerhof, Phys. Rev. Lett. **77**, 3865 (1996).

[43] M. Fuchs and M. Scheffler, Comput. Phys. Commun. **119**, 67 (1999).

[44] C. Huang and E. A. Carter, Phys. Chem. Chem. Phys. **10**, 7109 (2008).

[45] H. J. Monkhorst and J. D. Pack, Phys. Rev. B **13**, 5188 (1976).

[46] F. D. Murnaghan, Proc. Natl. Acad. Sci. U.S.A. **30**, 244. (1944).

[47] A. Stroppa, K. Termentzidis, J. Paier, G. Kresse, and J. Hafner, Phys. Rev. B **76**, 195440 (2007).

[48] J. P. Perdew and A. Zunger, Phys. Rev. B **23**, 5048 (1981).

[49] J. P. Perdew, R. G. Parr, M. Levy, and J. L. Balduz, Jr., Phys. Rev. Lett. **49**, 1691 (1982).

[50] M. J. Mehl, L. L. Boyer, and H. T. Stokes, J. Phys. Chem. Solids **57**, 1405 (1996); L. L. Boyer and M. J. Mehl, Ferroelectrics **150**, 13 (1993); L. L. Boyer, H. T. Stokes, M. M. Ossowski, and M. J. Mehl, Phys. Rev. B **78**, 045121 (2008).